PLASMONIC ENHANCEMENT OF ABSORPTION EFFICIENCY OF NANOPARTICLES FOR PHOTOTHERMAL THERAPY APPLICATIONS

by

Ege Şükrü Tahmaz

B.S., Mechanical Engineering, Boğaziçi University, 2019

Submitted to the Institute for Graduate Studies in
Science and Engineering in partial fulfillment of
the requirements for the degree of
Master of Science

Graduate Program in Mechanical Engineering
Boğaziçi University
2022

ACKNOWLEDGEMENTS

I dedicate this thesis to my late aunt Ayfer Dönmez, whose loss became the reason for my choosing this topic 3 years ago. If anything I studied or learned or did ever plays even an infinitesimal part in a solution that prevents someone from missing the birth of her grandson, I will be fulfilled.

I would like to express my endless gratitude to my thesis supervisor, Prof. Hakan Ertürk. I was honored to be someone he found worthy to share his brilliance with, but I am more grateful for his guidance, trust, and patience, even on days I was not sure I deserved it. I only hope that I can live up to the standards he set every day. I would also like to thank Assoc. Prof. Hasan Bedir and Prof. Kürşat Şendur for being a part of my thesis jury.

I cannot even begin to thank my mother, Aysen Tahmaz, and my father, Nihat Tahmaz for everything they ever did. They are the reason for everything I am and for everything I will be. I know that they are proud of me, and I feel their endless love. I can only try to be the son they deserve.

I also want to thank my close friends from Mongols: Ahmet Yavuz Demir, Barış Ege Sevgili, Gökberk Yaylalı, and Yiğit Korkmaz, for always being there. In times when I needed it the most, you tethered me down to reality, no matter how much I resisted it. From the moment we met for that barbeque all those years ago, you have affect everything I did. I hope I also had a positive effect on your lives, as that is what you deserve.

I would also like to thank Halil İbrahim Yazıcı, for being someone that I could complain about DDSCAT and someone I could turn to for help when I got stuck. When I was struggling with the user guide, it was comforting to know I was not alone.

ABSTRACT

PLASMONIC ENHANCEMENT OF ABSORPTION EFFICIENCY OF NANOPARTICLES FOR PHOTOTHERMAL THERAPY APPLICATIONS

Even though humanity is in a golden age when it comes to medical wonders, cancer is still one of the most common and deadly diseases in the world. One new treatment method is called photothermal therapy, which is the thermal ablation of cancer cells by the intravenous injection of plasmonic nanoparticles. Plasmonic nanoparticles absorb the incident light, converting almost all to heat, and increasing the temperature of the environment. But since the nanoparticles are taken intravenously, their placements in the tissue are randomized. In this thesis, the effects of adding dielectric nanoparticles to a plasmonic nanoparticle system on absorption are studied. Nanorods, nanocones, and bipyramid nanoparticles are considered as the dielectric nanoparticles due to their elongated shape. Effects of geometric parameters, such as the radius, on the absorption of the system are studied separately. Optimal parameters of each dielectric nanoparticle are identified. Multiple simulations are completed for each dielectric nanoparticle type where the nanoparticles is placed randomly in a control volume for an approximation of the randomly scattered nature of the nanoparticles in PTT. Nanocones are found to be the best dielectric nanostructure for improving absorption when the orientation of the dielectric nanoparticle can be controlled, with a 228.5% increase in absorption efficiency. However, the non-symmetric nature of the nanocone diminishes the absorption improvement greatly, with only a 68.1% improvement in absorption when the particles are placed randomly. Comparisons between the nanorods, nanocones and the bipyramid nanoparticles show that the slanted shaped dielectric nanoparticles are more suitable for PTT applications, while the symmetric geometry of the bipyramid nanoparticles provides more consistent improvements.

ÖZET

FOTOTERMAL TERAPİ KULLANIMI İÇİN NANOPARTİKÜLLERİN PLAZMONİK EMİLİM VERİMİNİN ARTTIRILMASI

İnsanlık medikal açıdan hiçbir zaman olmadığı bir noktada olmasına rağmen, kanser dünya üstündeki en yaygın ve ölümcül hastalıklardan biri olmaya devam etmektedir. Yeni bir tedavi olan fototermal terapi damar yoluyla enjekte edilip kanser hücresinde toplanan plazmonik nanopartiküllerin radyasyon yoluyla ısıtılması sonucuyla çevresindeki hücreleri öldürmesidir. Ancak nanopartiküller damar yoluyla verildiği için kanser hücresine nasıl yerleşeceği kontrol edilemez. Bu tezde, sisteme dielektrik bir nanopartikülün eklenmesinin plazmonik nanopartikül sisteminin emilim verilimi üstünde etkisi araştırılacaktır. Nanoçubuk, nanokoni, ikili nanopiramit uzun geometrileri nedeniyle bu amaçla kullanılan dielektrik parçacık türleridir. Bu parçacıkların yarıçapı gibi geometrik parametreleri emilim üstündeki etkileri tek başına anlaşılabilmesi için ayrı ayrı değiştirilmiştir. Her nanopartikül tipi için optimal geometrik parametreler seçilmiş, ve bu partiküller bir hacmin içinde rastgele yerleştirilmiştir. Nanopartiküllerin PTT kullanımında rastgele yerleşmesini modellemek için her nanopartikül şekli için birden fazla simulasyon yapılmıştır. Nanokonilerin emilim miktarını arttırmak için en verimli nanopartikül olduğu görülmüştür. Yerleştirmelerin önceden belirlendiği durumda emilim veriminde %228.5 bir artış olmasına neden olmuştur. Ancak nanokonilerin asimetrik şekilleri nedeniyle rastgele yerleştirilen durumda bu artış %68.1 değerine düşmüştür. Nanoçubuk, nanokoni ve ikili nanopiramit sonuçları karşılaştırıldığında ise eğimli parçacık geometrilerinin PTT için daha uygun olduğu, ve ikili nanopiramitin simetrik geometrisinin daha tutarlı bir artış sağladığı gözlemlenmiştir.

TABLE OF CONTENTS

ACKNOWLEDGEMENTS iii
ABSTRACT iv
ÖZET v
LIST OF FIGURES ix
LIST OF TABLES xii
LIST OF SYMBOLS xiv
LIST OF ACRONYMS/ABBREVIATIONS xv
1. INTRODUCTION 1
1.1. Cancer Treatment 1
1.2. Photothermal Therapy (PTT) 3
1.3. Nanoparticles 4
1.3.1. Nanoparticle Manufacturing 6
1.3.2. Types of Nanoparticles 6
1.3.2.1. Classification of Nanoparticles Based on Chemical Composition 6
1.3.2.2. Classification of Nanoparticles Based on Shape 8
1.4. Light Scattering and Absorption by Nanoparticles 9
1.4.1. Localized Surface Plasmon Resonance (LSPR) 10
1.4.2. Manipulation of Optical Properties of Plasmonic Nanoparticles . 11
1.4.2.1. Increasing Particle Size 11
1.4.2.2. Using Core-Shell Nanoparticles as Absorbers 12
1.4.2.3. Probing by AFM Tip 12
1.5. Objective of the Thesis 13
2. MODELING 15
2.1. Modeling Nanoparticle Systems 15
2.1.1. Modeling Incident Light 15
2.1.2. Modeling Optical Properties of Nanoparticles 15
2.1.3. Modeling Randomized Orientation 16

2.1.4. Modeling the Control Volume 17
2.1.5. Modeling Randomized Nanoparticle Placement 17
2.1.6. Modeling of Control Volumes as Absorbers 18
2.2. The Parameters of the Cancer Tissue 19
2.3. Nanoparticle Permeability of Cancer Tissue 20
2.4. Toxicology of the Nanoparticles 21
2.5. Dipole Generation of Each Nanoparticle 22
2.6. Cases Studied 24
2.6.1. Single Plasmonic Nanosphere Case 24
2.6.2. Two Plasmonic Nanospheres Case 25
2.6.3. Two Plasmonic Nanoparticles - One Dielectric Probe Case . . . 25
2.6.3.1. Nanosphere Probe Case 26
2.6.3.2. Nanorod Probe Case 26
2.6.3.3. Nanocone Case 27
2.6.3.4. Bipyramid Nanoparticle Case 28
2.6.4. Randomized Placement of Three Plasmonic Nanospheres - One Dielectric Nanostructure Case 28
3. METHODOLOGY 30
3.1. Generalized Lorenz-Mie Theory 30
3.2. Discrete Dipole Approximation 30
3.3. Comparison and Validation of Model 31
3.3.1. Single Au Nanosphere Results 31
3.3.2. Single SiO_2/Au Core-Shell Nanoparticle Results 32
3.3.3. Dipole Spacing 33
4. RESULTS AND DISCUSSION 36
4.1. Single Plasmonic Nanosphere 36
4.2. Two Plasmonic Nanospheres 38
4.2.1. Changing the Plasmonic Nanosphere Sizes Concurrently 38
4.2.2. Changing the Plasmonic Nanosphere Sizes Separately 39
4.3. Two Plasmonic Nanospheres with One Dielectric Nanoparticle 41
4.3.1. Nanosphere Case 41

4.3.2. Nanorod Case 43
4.3.2.1. Changing the Length h_r of the Nanorod 43
4.3.2.2. Changing the Radius r_r of the Nanorod 44
4.3.3. Nanocone Case 46
4.3.3.1. Changing the Length h_c of the Nanocone 46
4.3.3.2. Changing the Tip Radius r_{tip} of the Nanocone 47
4.3.3.3. Changing the Tip Angle β of the Nanocone 48
4.3.4. Bipyramid Nanoparticle Case 49
4.3.4.1. Changing the Length h_b of the Bipyramid Nanoparticle 49
4.3.4.2. Changing the Tip Radius $r_{tip,b}$ of the Bipyramid Nanoparticle 51
4.4. Randomized Placement of Three Plasmonic Nanospheres - Single Dielectric Nanostructure Case 52
5. CONCLUSION 57
REFERENCES 60
APPENDIX A: DIPOLE PLACEMENT FOR DIFFERENT NANOPARTICLE SHAPES 75
A.1. Nanospheres 75
A.2. Nanorods 75
A.3. Nanocones 76
A.4. Bipyramid Nanoparticles 77

LIST OF FIGURES

1.1 Localized Surface Plasmon Resonance. 11

2.1 Complex Refractive Index m of Commonly Used Nanoparticle Materials, data taken from: silicon [81], silica [82], silicon nitride [83], gold [84], silver [84]. 16

2.2 (a) Placement Centers in Controlled Volume, and (b) Finalized Placement by Normalized Distribution 17

2.3 Histogram of Distances Between (a) Two Plasmonic Nanoparticles ($\mu = 3.755, \sigma = 0.523$), and (b) a Plasmonic Nanoparticle and a Dielectric Probe ($\mu = 2.484, \sigma = 0.685$) in 100 Randomized Placements. 18

2.4 Dipoles of (a) a Nanosphere ($r_s = 10nm$), (b) a Nanorod ($r_r = 10nm, h_r = 60nm$), (c) a Nanocone ($r_{tip} = 10nm, h_c = 60nm, \beta = 10°$), (d) a Bipyramid Nanoparticle ($h_b = 120nm, r_b = 20nm, \beta = 30°$). 23

2.5 Dipoles Included in a Height z. 24

2.6 The Configuration of Two Plasmonic Nanospheres. 25

2.7 The Configuration of Nanosphere Case. 26

2.8 The Configuration of Nanorod Case. 27

2.9 The Configuration of Nanocone Case. 27

2.10 The Configuration of Bipyramid Nanoparticle Case. 28

2.11 Placement Examples for Three Plasmonic Nanospheres ($r_s = 10nm$, shown in blue) and One Dielectric Nanorod ($r_r = 10nm, h_r = 100nm$, shown in red). 29

3.1 Rectangular Object Separated into Dipoles. 31

3.2 C_{abs} Comparison of a single Au nanosphere. 32

3.3 C_{abs} Comparison of a SiO_2/Au Core-Shell Nanoparticle. 32

3.4 Comparison of (a) Q_{abs} and (b) Q_{sca} for a Single Au Nanosphere ($r = 20nm$) with Changing Interdipole Spacing d. 34

4.1 Q_{abs} of Single Au Nanosphere with Changing Radius r_s. 36

4.2 Q'_{abs} of Single Au Nanosphere with Changing Radius r. 37

4.3 Q_{abs} of Two Au Nanospheres with Changing Radii r. 38

4.4 $Q_{abs}/Q_{abs,0}$ of Two Au Nanospheres with Changing Radii r_s. . . . 39

4.5 Q_{abs} of Two Au Nanospheres with Different Radii and the Equivolumetric System (a) $r_1 = 10nm, r_2 = 20nm$, (b) $r_1 = 10nm, r_2 = 30nm$, and (c) $r_1 = 20nm, r_2 = 30nm$. 40

4.6 Q'_{abs} of a System with SiO_2 Nanosphere with Changing Probe Radius $r_{s,d}$. 42

4.7 Q'_{abs} of a System with SiO_2 Nanorod with Changing Rod Length h_r. 43

4.8 Q'_{abs} of a System with SiO_2 Nanorod with Changing Rod Radius r_r. 45

4.9 Q'_{abs} of a System with SiO_2 Nanocone with Changing Probe Length h_c. 46

4.10 Q'_{abs} of a System with SiO_2 Nanocone with Changing Tip Radius r_{tip}. 47

4.11 Q'_{abs} of a System with SiO_2 Nanocone with Changing Probe Tip Angle β. 48

4.12 Q'_{abs} of a System with SiO_2 Bipyramid Nanoparticle with Changing Bipyramid Nanoparticle Length h_b. 50

4.13 Q'_{abs} of a System with SiO_2 Bipyramid Nanoparticle with Changing Bipyramid Tip Radius $r_{tip,b}$. 51

4.14 Q'_{abs} of a System with Two Au Nanospheres and Single SiO_2 Nanostructure in Prescribed Positions, Nanocone ($r_c = 5nm, h_c = 60nm, \beta = 10°$), Nanorod ($r_r = 5nm, h_r = 60nm$), Bipyramid Nanoparticle ($r_b = 5nm, h_c = 60nm, \beta = 10°$). 53

4.15 Averaged Q'_{abs} ($average \pm 5\%$) of a System with Three Au Nanospheres and One SiO_2 Probe in Randomized Positions; Nanocone ($r_{tip} = 5nm, h_c = 60nm, \beta = 10°$), Nanorod ($r_r = 5nm, h_r = 60nm$), Bipyramid Nanoparticle ($Sharp\ Tip, h_c = 60nm, \beta = 10°$). 54

A.1 Geometric Representation of a Nanosphere. 75

A.2 Geometric Representation of a Nanorod. 76

A.3 Geometric Representation of a Nanocone. 77

A.4 Geometric Representation of a Bipyramid Nanoparticle. 78

LIST OF TABLES

2.1 Refractive indexes of cancer tissue in different places in the human body. 19

2.2 Nanotoxicological Effect of Most Commonly Used Nanoparticle Materials. 21

3.1 Maximum allowed interdipole spacing for the materials used in the thesis. 33

3.2 Simulation times and the LSPR peaks of different interdipole spacings in modeling a single Au nanosphere ($r = 20nm$). 35

4.1 Effects of changing the radius of dielectric nanosphere, r_s on absorption. 42

4.2 Effects of changing the length of dielectric nanorod, h_r on absorption. 44

4.3 Effects of changing the radius of dielectric nanorod, r_r on absorption. 45

4.4 Effects of changing the length of dielectric nanocone, h_c on absorption. 47

4.5 Effects of changing the tip radius of dielectric nanocone, r_c on absorption. 48

4.6 Effects of changing the tip angle of dielectric nanocone, β on absorption. 49

4.7 Effects of changing the length of dielectric bipyramid nanoparticle, h_b on absorption. 50

4.8 Effects of changing the tip radius of dielectric bipyramid nanoparticle, $r_{tip,b}$ on absorption. 52

4.9 Average improvement of energy absorbed by the addition of probes. 55

LIST OF SYMBOLS

a_{eff}	Effective radius of the system
a_{plas}	Effective radius of the plasmonic nanoparticles
C_{abs}	Absorption cross-section
C'_{abs}	Absorption cross-section per plasmonic nanoparticle volume
d	Interdipole
d_s	Distance between the plasmonic nanospheres
d_p	Distance between the dielectric nanoparticle and the plasmonic nanospheres
h_b	Length of the dielectric bipyramid nanoparticle
h_c	Length of the dielectric nanocone
h_r	Length of the dielectric nanorod
m	Complex refractive index
$r_{tip,b}$	Tip radius of the dielectric bipyramid nanoparticle
r_c	Tip radius of the dielectric nanocone
r_r	Tip radius of the dielectric nanorod
r_s	Radius of the plasmonic nanosphere
$r_{s,d}$	Radius of the dielectric nanosphere
Q_{abs}	Absorption efficiency
Q'_{abs}	Absorption efficiency with respect to plasmonic nanoparticle size
β	Nanocone tip angle

LIST OF ACRONYMS/ABBREVIATIONS

0-D	Zero Dimensional
AFM	Atomic force microscopy
DDA	Discrete dipole approximation
EPR	Enhanced permeability and retention
LSPR	Localized surface plasmon resonance
PTT	Photothermal therapy
PTA	Photothermal agents

1. INTRODUCTION

1.1. Cancer Treatment

The progression in medical research in recent years greatly improved the treatments for some of the most dangerous diseases into world or discovered cures for previously incurable diseases. But with all of the advancements in medicine, cancer treatment remains one of the least effective, and most dangerous treatments for a disease that affects the general population as much as cancer does. World Health Organization (WHO) estimates the annual cancer cases to rise from 14 million to 22 in the span of two decades [1]. The uncontrollable division and accelerated growth of tumor cells are the primary reasons for the challenges of the treatments [2]. While the current methods of treatment such as surgery, chemotherapy, and radiation therapy have different levels of success rates, each treatment method has its drawbacks. For cancer tissue that can be easily accessible, and is local to a single area; surgery is the recommended procedure because of its high success rate in either complete removal of the tumor, or the reduction of the tumor's size [3]. Metastasized cancer cannot be treated by surgery, therefore the surgical option is generally used for cancer in the early stages. Chemotherapy treats cancer by attacking active cells, cells that are growing and dividing. The potent drugs used in chemotherapy damage active cells severely, both cancer and healthy cells. This targeting of healthy cells has both short-term effects like nausea, hair loss, and compromised immune system; and long-term effects like blood disorders, and nerve damage [4–6]. Deaths of other diseases because of the compromised immune system are also common in patients treated with chemotherapy [7]. Radiation therapy is the targeted DNA-damaging of the cancer cells by continuous high-dosage radiation. While cancer cells are more greatly affected by the incident radiation because of their rapid cell division, healthy cells are also affected similarly to chemotherapy [8]. Side effects of radiotherapy are relatively mild compared to chemotherapy, but the treatment success of the method is also lower. Therefore, radiotherapy is generally administered in conjunction with a different treatment [9,10]. Even though these treatments are used in most cancer cases, other state-of-the-art methods of treatment with higher success rates or usable in more challenging cases are researched.

The advancements in nanotechnology allow for a more precise approach to cancer treatment. The tunability of nanoparticles and their relatively large surface areas make them an excellent agent for transportation. Most treatments involving nanoparticles primarily rely on the enhanced permeability and retention (EPR) effect of tumor tissue which defines the nanoparticle accumulation in the tumor tissue [11]. Since the permeability of the tissue is affected by many different characteristics of the tumor, different cancers all have different size limits for the nanoparticles absorbed [12]. The precision of the treatment is also increased by controlling the triggering events of the treatment, usually electromagnetic waves.

Many studies aim to use nanotechnology to enhance current treatments. For example, targeted drug delivery using nanocarriers are a proposed method of improvement to chemotherapy. The side effects of drug treatment are minimized by transporting the drugs by nanostructures which are activated when exposed to light in a specific wavelength, usually in the visible or near-infrared (NIR) range. By releasing the chemotherapeutic drugs much closer to the tumor tissue, the drug's overall therapeutic index is also increased [13, 14]. Similarly, studies about improving radiotherapeutic treatment by the introduction of nanoparticles as radiosensitizers into the tumor tissue show promising results. Since radiotherapy is limited by the degeneration of healthy cells because of the incident radiation, decreasing the radiation dosage or augmenting the therapy itself vastly improves the viability of the treatment [15].

The emergence of nanoparticles in medicine has not only improved pre-existing treatments; it has also allowed for new methods of treatment to be developed and improved. For example, nanoparticles are now commonly used in photodynamic therapy (PDT) applications where their inclusion as transporters exhibit great improvements in efficacy compared to cases where other photosensitizers are used [16, 17]. Immunotherapy is a bleeding-edge treatment using the patient's immune system and promoting new immune cell development to eradicate or shrink the tumor tissue [18]. Nanotechnology is used to both identify the tumor cells to better understand what type of immune response is going to be stimulated by external factors for treatment.

Nanoparticles are most commonly used as a method of targeted delivery of different components in cancer treatment [19]. But the radiation absorbing capabilities of the nanoparticles, that is frequently used to stimulate the release of a component in the desired location can also be used as a heating mechanism. The state-of-the-art treatment method that is reliant on the aforementioned heating mechanism is called photothermal therapy (PTT). This method of treatment is explained in detail in the following section.

1.2. Photothermal Therapy (PTT)

Unlike the cancer treatments mentioned in Section 1.1, PTT is a non-invasive method that aims to eliminate tumor tissue by thermal ablation [20–22]. Similar to PDT, photothermal agents (PTA) are administered to the patient, most commonly by intravenous injection. Electromagnetic waves are focused on the primary cancer site after a predetermined time because of the varying permeability of different cancers. PTAs that are randomly scattered throughout the tumor absorbs incident radiation, heating the neighboring tumor tissue and promoting preferable cell death of the cancer cells [23].

There are two different types of cell death that is induced by hyperthermia, necrosis, and apoptosis [24]. Necroptic cells are cells that have ruptured cell membranes whose contents are released into the medium [25]. Apoptotic cells are still functional cells which are divided into much smaller parts. These cells are then destroyed by the immune system of the host [26]. Both cell death mechanisms can be promoted by PTT, depending on the irradiation incident on the PTAs. Necrosis is induced by a fast temperature increase of the cells to $> 50°C$, while apoptosis is achieved by maintaining a temperature of $43 - 50°C$ for an extended period [24].

Many different types of PTA can be used in PTT. For example, dye molecules like indocyanine green can be used because of their high absorption cross-sections and photothermal efficiency [27, 28]. This increase greatly reduces the irradiation required to damage the diseased tissue; therefore, reducing the side effects of the operation. While dye molecules have desirable properties for PTT usage, the continued usage of the dye is severely limited by photobleaching, a non-reversible process of deterioration [27]. Therefore, plasmonic nanoparticles (NP) are primarily used as PTAs [20,22,29,30] because of their high tunability, and much higher absorption cross-sections compared to dye molecules. These NPs are highly stable and are not affected by photobleaching, which makes them resistant to deterioration. The accumulation of the NPs in the cancer tissue is detailed in Section 1.1. Gold (Au) NPs are primarily used because of their biocompatibility and high light-to-heat conversion. Even though Au in its bulk state is completely non-toxic, there is evidence to suggest some toxicity in the nanoscale. The toxicity of the NPs is also a limiting factor in how much of a single material can be administered to the patient without serious side effects. This limitation makes the research on increasing the absorption of light while keeping the PTA volume constant important.

1.3. Nanoparticles

Nanotechnology as a field of study has gained popularity in recent years because of developments in manufacturing that allow for complex structures to be created in much smaller sizes. Nanotechnology can be defined as processes and operations done at the nanoscale (sizes between $1 - 100nm$). Richard Feynman proposed the concept of nanotechnology in his famed lecture *"There is Plenty of Room at The Bottom"* [31]. However, the first mention of nanotechnology came from Norio Taniguchi, a Japanese scientist who used it the describe a semi-conductor in the nanoscale [32]. These concepts were expanded upon by Drexler [33] when he described an imaginary machine in the nanoscale that had the ability of assembling nanoscale structures, which could be other copies of the original machine or new components, marking the first proposal of automation in the nanoscale. Even though nanotechnological advancements have only recently reached this proposed level of complexity, nanotechnology has been used in many industrial applications, such as manufacturing of nanoelectronics [34,35], improvement of durability in clothing items [36], improvement of efficiency in solar cells [37–39], and biomedical applications like imaging and targeted drug delivery [35,40,41].

Nanoparticles can be seen as the building blocks of nanotechnology. A nanoparticle was originally defined as a singular structure that has dimensions at the nanoscale, but this definition has since expanded to include any material that has at least one dimension at the nanoscale. Structures that have all three dimensions (x, y, z) in the nanoscale can be more accurately defined as zero-dimensional (0-D) nanoparticles. Likewise, materials that have a single dimension and two dimensions that exceed the nanoscale are called one-dimensional (1-D) and two-dimensional (2-D) nanoparticles, respectively [42].

Nanoparticles tend to have drastically different optical properties when compared to bulk materials because of their increased surface area-to-volume ratio. In the nanoscale, a larger percentage of the atoms in a particle is located in the surface layer, which is defined as a layer 5 atoms thick. Therefore, the properties of the surface layer dominates over the properties of the bulk material, allowing for the atomic structures of the material to have a larger effect on the properties of the structure. For example, nanoparticles are much more efficient heat absorbing and transferring structures compared to larger structures like microparticles, which have dimensions between $1 - 100\mu m$, as the interactions between the surface atoms and the incident electromagnetic waves dictate how the nanoparticle behaves when an electromagnetic wave is incident upon it [43]. A larger percentage of atoms in the surface layer allow for a larger portion of the atoms in a nanoparticle to interact with the incident light, scattering some portion of light away while converting another portion of light into heat, or absorbing light, if the nanoparticle is composed of a light absorbing material. The scattering and absorbing behaviour of nanoparticles irradiated by electromagnetic waves form the basis of nanophotonics and are used extensively in many fields, such as electrical engineering, renewable energy, and biomedicine. Absorption and scattering phenomena are explained in detail in Section 1.4.

1.3.1. Nanoparticle Manufacturing

While there are many different methods for manufacturing nanoscale structures, most of these methods can be defined as "top-down" or "bottom-up" approaches [44]. Top-down methods or destructive methods are the diminishings of bulk materials into nanoscale particles. Since most top-down methods are mechanical processes that require great precision, manufacturing small or complex nanoparticles with these methods is challenging. The most commonly used top-down manufacturing method is mechanical milling, where a bulk material is ground down to nanoparticles [45]. Bottom-up or constructive methods are defined as the clustering of atoms into nanoparticles. These methods are more complex and time-consuming but allow for the manufacturing of more complex nanoparticles like core-shell nanoparticles or nanostars with a higher level of control. For example, the most commonly used bottom-up manufacturing process, the sol-gel method, is a multi-step chemical and thermal process [46].

1.3.2. Types of Nanoparticles

Because of the highly variable nature of their properties, there are many different parameters used when classifying nanoparticles. These classifications include but are not limited to the manufacturing method, origin, composition, size, shape, and area of application [42]. Since composition and shape are some of the most commonly changed variables and the parameters of which the effects are studied in this thesis, these classifications will be further discussed.

1.3.2.1. Classification of Nanoparticles Based on Chemical Composition.

- Metal Nanoparticles: Metal nanoparticles are homogeneous nanoparticles that are composed of metallic elements. The most common types of metal nanoparticles include gold (Au), silver (Ag), copper (Cu), and platinum (Pt) [47]. These nanoparticles are excellent scatterers and absorbers. The reasoning behind this phenomenon is explained in Section 1.4.1. Because of their highly tunable and unusual optical properties, metal nanoparticles are the most commonly used type of nanoparticle in industrial applications [48]. In biomedical applications, noble metal nanoparticles have low toxicity that makes them suitable for biological imaging and treatment [49].

- Silica-Based Nanoparticles: Silica-based nanoparticles are nanoparticles composed of silicon (Si) or silica (SiO_2). Silica-based nanoparticles are mostly used in biomedical applications because of their bio-compatibility [50]. Since most silicon compounds are dielectrics, silica-based nanoparticles usually are poor light absorbers but provide improvements in electric and magnetic fields [51].
- Metal Oxide Nanoparticles: Metal oxide nanoparticles are composed of oxidized metals. Most common metal oxide nanoparticles include tin oxide (TiO_2), zinc oxide (ZnO), and copper oxide(CuO). Metal oxide nanoparticles can have conducting, semi-conducting, or insulating properties [52]. Metal oxide nanoparticles exhibit similar optical properties to metal nanoparticles because of their similarities in molecular structure, in particular their large electron clouds.
- Carbon-Based Nanoparticles: Carbon-based nanoparticles are nanoparticles created by different arrangements of mostly carbon atoms. Because of the strong bonds between carbon atoms, carbon-based nanoparticles have extremely high stability [53]. Even though carbon-based nanoparticles have extremely high thermal and electrical conductivities, carbon-based nanoparticles are not used extensively in biological applications. But the high tunability of these nanoparticles allow for different nanoparticles to be manufactured that are better suited for certain tasks, for example carbon nanotubes that have higher solubility in water for PTT usage [54].
- Organic Nanoparticles: Organic nanoparticles are nanoparticles that are composed of organic molecules like liposomes, and protein strands. Organic nanoparticles are both naturally observed and manufactured. Because of their biodegrad-

ability and relative ease of usage in encapsulation, most targeted drug delivery research focuses on organic nanoparticles [55].

1.3.2.2. Classification of Nanoparticles Based on Shape.

- Nanospheres: Nanospheres are homogeneous spherical nanoparticles. Nanospheres are the most commonly used nanoparticle, mostly because of their ease of manufacturing and the large surface area-to-volume ratio [47]. The optical properties of the nanospheres are dependent on their radius and composition.
- Core-Shell Nanoparticles: Core-shell nanoparticles or composite nanoparticles are a combination of a core section inside a hollow shell section composed of a different material. While spherical two-material core-shell nanoparticles are most common, three-material core-shell nanoparticles or core-shell nanoparticles with different shapes can also be manufactured [56]. Core-shell nanoparticles gained popularity in research because of their high tunability. Core-shell nanoparticles demonstrate improved plasmonic properties compared to homogeneous nanospheres. The optical properties of the core-shell nanoparticles are dependent on the shell thickness, core radius, and core and shell materials [57].
- Nanorods: Nanorods are rod-shaped nanoparticles. Both ends of the nanorods can be approximated as hemi-spheres. The optical properties of nanorods are affected by the radius of the rod, and more importantly the aspect ratio. Plasmonic nanoparticles have two LSPR peaks, longitudinal and transverse [58]. Because of their elongated shape, the orientation of the nanorods with respect to the incident electric field affects the optical properties of the nanomaterial. Nanorods have many applications, from targeted drug delivery [59] to light emitting [60].
- Nanocones: Nanocones are cone-shaped nanoparticles. The base diameter and length of the nanocone have dimensions in the same order of magnitude, separating them from nanowires. Nanocones are mostly used in solar cell technology for increased light absorption by trapping [61].

- Nanopyramids: Nanopyramids are pyramid-shaped nanoparticles. AFM tips are usually nanopyramids [62]. Nanopyramid arrays are also used in solar cells for their light trapping capabilities [63].
- Bipyramid Nanoparticles: Bipyramid nanoparticles can be defined as two nanopyramids or nanocones joined at the base. Plasmonic bipyramid nanoparticles also exhibit two LSPR peaks, one longitudinal and one transverse [64], similar to nanorods. These nanoparticles are primarily used in diagnostics [30] and photothermal therapy [65] applications.

1.4. Light Scattering and Absorption by Nanoparticles

In PTT, monochromatic unpolarized light is used in order to promote localized heating around the nanoparticle. In order to understand the principles of PTT, it is crucial to understand the phenomena that occur when monochromatic unpolarized light hits a nanoparticle. The first phenomenon is scattering, where the incident light is either refracted or reflected in different directions. The total scattering is an amalgamation of two different types, elastic and inelastic scattering. Inelastic scattering, also called Raman scattering in nanoparticles, defines a type of scattering where the energy of the incident light also changes after the collision between the light and the nanoparticle [66]. While typically a very small amount of scattering is inelastic, the usage of plasmonic nanoparticles or an electric field improvement around the nanoparticle can promote a larger quantity of inelastic scattering. The polarization change in the scattered light is generally used for identification purposes in a process called surface-enhanced Raman spectroscopy (SERS). However, most of the incident light undergoes elastic scattering, that is referred to as Rayleigh scattering in cases where nanoparticles are much smaller than the incident wavelength, as in the case of nanoparticles.

The other phenomenon that occurs when light hits a particle is called absorption, where the incident light is converted into thermal energy. While every particles scatters incident light, absorption occurs under some circumstances [67]. Light absorbing materials can be classified by their complex refractive index m. m is defined by

$$m = n + ik, \tag{1.1}$$

where n is the refraction index, and k is the absorption index.

The absorption and scattering processes result in a decrease in the energy of the incident light beam. This total decrease is called extinction. In non-symmetric structures, it is possible that different polarizations have different extinction coefficients. Therefore, the scattered light might have a different polarization state than the incident light. This phenomenon is called dichroism [68]. The absorbed and scattered light is expressed in absorption and scattering cross-sections, C_{abs} and C_{sca} respectively. These cross-sections represent the probability of absorption or scattering and can be converted into radiant flux by

$$\Phi_{e,x} = E_e C_x, \tag{1.2}$$

where $\Phi_{e,x}$ denotes the scattered or absorbed radiant power, E_e denotes the incident irradiance, and C_x denotes the scattering or absorption cross-section.

1.4.1. Localized Surface Plasmon Resonance (LSPR)

The most important property of metal nanoparticles and the major reason behind the research interest in using them is their free electrons, which allow for free electron oscillations on the surface of the particle. This phenomenon is called a surface plasmon (SP), and it only occurs at the interfaces between metal and dielectric materials [69, 70]. Because of this property, metal nanoparticles are also called plasmonic nanoparticles. In nanoparticles that are smaller than the wavelength, when light is directed to the nanoparticle, these SPs become periodic and orderly, becoming localized surface plasmons (LSP). The existence of LSPs greatly enhances the electric fields around the nanoparticles, making plasmonic nanoparticles excellent absorbers. LSPs are greatly affected by particle size, particle and environment refractive indexes, and the incident wavelength. Light waves become entrapped within the nanoparticle at a specific wavelength that is dependent on the material, shape, and size of the nanoparticle. This phenomenon is called localized surface plasmon resonance (LSPR) and can be seen in Figure 1.1. Nanoparticles in LSPR exhibit enhanced optical properties. The absorption cross-section of the nanoparticle reaches its maximum, and almost all scattered light is in Rayleigh scattering [71]. Because of these properties, most research on plasmonics focuses on LSPR regions.

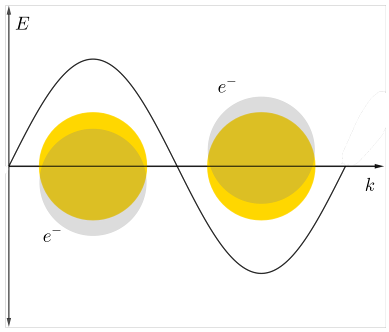

Figure 1.1: Localized Surface Plasmon Resonance.

1.4.2. Manipulation of Optical Properties of Plasmonic Nanoparticles

The optical properties of plasmonic nanoparticles are extremely tunable. In PTT, the absorption of the incident light, and the LSPR region are one of the most important properties to control. As nanoparticles display optimal optical properties in the LSPR region, methods for adjusting the LSPR wavelength are crucial [72]. The absorption property of plasmonic nanoparticles can also be enhanced with many different methods. Some methods involve the alteration of the absorbing nanoparticles, while other methods enhance the electric field around the nanoparticle by external additions. These methods are explained in this section with the plausibility of their applications in PTT.

<u>1.4.2.1. Increasing Particle Size.</u> As the size of the particle increases, an increase in the plasmonic extinction peak can be observed because of the change in the surface area of the nanoparticle. But since extinction is a combination of scattered and absorbed

light, an increase in the extinction efficiency does not connote an increase in the absorption efficiency in the nanoparticle. The size dependence of the absorption efficiency of plasmonic nanoparticles does not follow a linear relation. El-Sayed and Link [73] experimentally presented a redshift in LSPR peaks of gold spherical nanoparticles as radius r increases. Chang et al. [74] show a linear relation between the absorption and nanoparticle volume, while the scattering scales with volume squared. After a certain size where scattering becomes the main mode of extinction, the absorption of light decreases even though the total extinction of light increases. This phenomenon can be attributed to the dominance of scattering in nanoparticles as the size of the nanoparticle approaches the wavelength of the incident light.

1.4.2.2. Using Core-Shell Nanoparticles as Absorbers. Core-shell nanoparticles are briefly explained in Section 1.3.2.2. Dielectric core-metal shell nanoparticles are primarily used as photothermal agents, and optical contrast agents because of their high LSPR tunability, allowing the peak to be in the near-infrared (NIR) region. LSPR peak in the NIR region is desirable, because of increased transmission of incident light through tissue. Yu et al. [75] show a redshift in the LSPR peak when shell thickness, t_{shell}, increases while keeping core diameter, d_{core}, constant. An increase in the absorption efficiency Q_{abs} can be observed as t_{shell} increases. Metal core-dielectric shell nanoparticles have higher physical and chemical stabilities compared to solid plasmonic nanoparticles [56]. These nanoparticles also demonstrate enhanced plasmon resonances because of the surface interactions between core and shell materials. Yu et al. [75] also shows an increased scattering/absorption q_{sca}/q_{abs} ratio in metal-dielectric particles when comparing dielectric-metal and metal-dielectric core-shell nanoparticles .

1.4.2.3. Probing by AFM Tip. Atomic Force Microscopy (AFM) is an extremely sensitive method of surface imaging, with resolutions in the nanometer scale. A microscale probe is attached to a reflective cantilever whose upper surface is irradiated by a laser. As the AFM probe moves over the surface, the cantilever is bent as the sharp tip contacts the surface changing the amount of reflected laser beam onto a sensor. Then the movement of the AFM probe tip is calculated from the changes in the amount of reflected laser [76]. While the tips of the AFM probe is in the nanoscale, the entire structure is too large to be classified as a 0-D nanoparticle.

An important property of the AFM tips in regards to plasmonics is the improved absorption efficiency of plasmonic nanoparticles when an AFM tip is in close proximity. This phenomenon occurs due to the near-field coupling between the tip of the AFM probe and the nanoparticle, promoting improved absorption in the plasmonic nanoparticle. The improvement of absorption brought about by the inclusion of the AFM probe can be further increased by the optimization of different system parameters. Huda et al. [77] studied the absorption efficiencies of Au and Ag nanoparticles when Au and Si probes are placed near them. Even though Si AFM probes do not absorb incident light, using of these probes still improves the absorption efficiency of the system. Conversely, the systems with Au probes have a higher total absorption rate, but the absorption of the plasmonic nanoparticles suffer from the addition of these probes. Talebi et al. [78] compared the increase in the absorption efficiency when a dielectric probe is placed near solid Au nanoparticles and $SiO_2 - Au$ core-shell nanoparticles. The results show that the addition of the SiO_2 core promoted the enhancement of absorption and a more uniform absorption. Talebi et al. [79] also studied the effect of Si probe placement on the absorption by an array of Au nanospheres irradiated by a surface evanescent wave placed on a borosilicate glass surface. The results of this study show that the local absorption of the nanospheres can be enhanced or reduced by the placement of the Si tip, providing precision in localized heating. Avşar et al. [80] studied GaP and Si as tip materials, and compared the effects of introducing an dielectric external tip and showed that GaP tips provide better enhancement in absorption, proving that the absorption efficiency is dependent on the refractive index of the dielectric material.

1.5. Objective of the Thesis

The results presented in the aforementioned studies show the potential of 'probing' in PTT. The main difference with the application of 'probing' in a therapeutic method like PTT is the length of the probes and the lack of a surface. The probe length in these studies is always taken to be relatively infinite compared to the nanoparticles. Therefore, these probes can be characterized as 1-D or 2-D nanoparticles. Since these probes have lengths in the micrometer scale, they are too large for them to be positively affected by the increased permeability of the cancer tissue, called the EPR effect, and therefore cannot be introduced to the cancer tissue in the same manner as the plasmonic nanoparticles. Another difference from the existing literature is the randomized positioning and orientation of the nanoparticles when injected intravenously, while almost every study regarding AFM probes has tightly controlled positioning and orientations for the probe and the nanoparticles. The enhancement of absorption in plasmonic nanoparticles when dielectric elongated nanoparticles are introduced to the system instead of AFM tips is still not well known. The research on the enhancement of absorption with the introduction of AFM tips mostly focuses on an array or a singular plasmonic nanoparticle placed upon a substrate, which is not possible in PTT applications. Similarly, while the effects of the composition of the tip is well-known, the shape of the dielectric particle is not studied. Therefore, the current knowledge in literature is not enough to correctly predict if a homogeneous mixture of plasmonic nanoparticles and dielectric nanoparticles can be an improvement in PTT when compared to the current method of using a single type of nanoparticle. This thesis aims to study the effects of adding a dielectric nanostructure into a randomly placed plasmonic nanoparticle system on the absorption of the system for PTT usage.

In this thesis, the modeling of the nanoparticle systems is described first. The boundary conditions, like the nanoparticle toxicities and the largest nanoparticle that could be absorbed into the cancer tissue, and the geometries of the different types of nanoparticles used in the study are defined. Then, the cases studied are described. The geometric parameters of the systems are first studied in systems with prescribed positions for shorter simulation times. The methodology used in the thesis is described next with validation studies also presented. Lastly, the results from the aforementioned cases are presented, from the simplest case to the randomized cases.

2. MODELING

2.1. Modeling Nanoparticle Systems

Because of the size difference between the nanoparticles and the cancer tissue, models must be simplified for computational simulations to be possible. Therefore, the existence of the cancer tissue is ignored and the particle system is assumed to be in free space with an medium refractive index similar to cancer tissue. In this section, these simplifications are explained.

2.1.1. Modeling Incident Light

The properties of light used in PTT are briefly mentioned in Section 1.4. For computational calculations, the polarization state of the incident light must be defined. Therefore, unpolarized light is modeled as the average of two perpendicularly polarized light states. The two light beams are polarized on the y-axis and z-axis. Since the scattering and absorption of light by nanoparticles are dependent on the polarization of the light, dichroism, briefly explained in Section 1.4 can be overestimated as the unpolarized light is modeled by only two polarized light beams.

2.1.2. Modeling Optical Properties of Nanoparticles

The complex refractive index of the nanoparticles is mostly different from the bulk material and is dependent on the incident wavelength. Spectral optical properties for materials commonly used in the literature is presented in Figure 2.1.

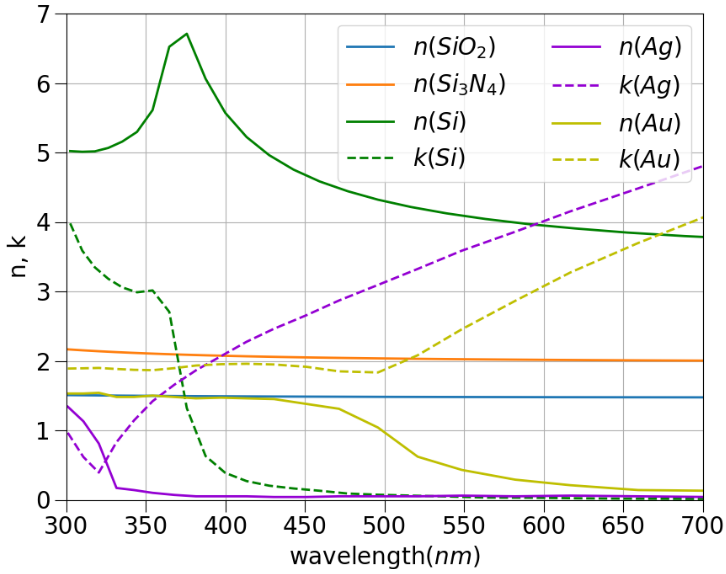

Figure 2.1: Complex Refractive Index m of Commonly Used Nanoparticle Materials, data taken from: silicon [81], silica [82], silicon nitride [83], gold [84], silver [84].

It can be seen that the relationship between incident wavelength and the refractive index is linear in dielectric nanoparticles. Plasmonic nanoparticles have complex refractive indexes, with n values decrease when the wavelength of the incident light increases, while k values are inversely related to the wavelength. In this study, the composition of the plasmonic nanoparticles is chosen to be Au, while the dielectric nanoparticles are chosen to be SiO_2 because of its low toxicity and common usage in the field of nanophotonics.

2.1.3. Modeling Randomized Orientation

Considering the randomized placement of a number of nanoparticles, the angle at which light is incident system can result in a change in the optical properties of the system. Therefore, the results of the system must be orientationally averaged. The user guide for DDSCAT suggests 500 different orientations for each system are to be calculated and averaged [85]. This averaging is assumed to result in a satisfactory averaging with no bias.

2.1.4. Modeling the Control Volume

The control volume at which the nanoparticles will be suspended in is referred to as the environment or the medium. The environmental data of the refractive index m is taken from Table 2.1 in Section 2.2. Even though tissue has an inherently heterogeneous composition, the environment is assumed to be homogeneous. A safety gap is defined in the control volume. This gap is placed around the control volume to minimize the effects of absorption from the neighboring control volumes, as this effect can not be simulated by DDSCAT. Ivezic and Mengüç suggest that a distance of $3r$ for spherical nanoparticles is satisfactory [86]. Since the aim is to minimize the interparticle effects between two neighboring control volumes, a safety gap of $\frac{3r_{plas}}{2}$ is placed in every control volume. The dimensions of the control volume are considered as $200nm$ x $200nm$ x $200nm$.

2.1.5. Modeling Randomized Nanoparticle Placement

A homogeneous placement of nanoparticles in the environment is assumed. This homogeneous placement is modeled as nanoparticles placed around on equidistant placement centers in the control environment. To simulate randomized placing, the exact positioning of the nanoparticle around the placement center is determined by normalized distribution. Figure 2.2 show a representation of the placement centers and normalized distributions of the nanoparticles.

(a) (b)

Figure 2.2: (a) Placement Centers in Controlled Volume, and (b) Finalized Placement by Normalized Distribution

The orientations of each particle are also randomized. The histograms of particle distances between two nanoparticles, and a particle and a probe are presented in Figures 2.3a and 2.3b respectively.

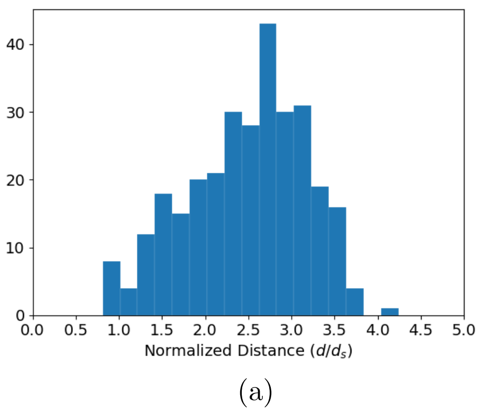

Figure 2.3: Histogram of Distances Between (a) Two Plasmonic Nanoparticles ($\mu = 3.755, \sigma = 0.523$), and (b) a Plasmonic Nanoparticle and a Dielectric Probe ($\mu = 2.484, \sigma = 0.685$) in 100 Randomized Placements.

30 different placements are deemed satisfactory for homogeneity calculations, as 30 is the conventional number of samples for accurate statistical results.

2.1.6. Modeling of Control Volumes as Absorbers

The plasmonic particles are the main absorbers in the system. But it is computationally challenging to measure the absorption of each nanoparticle with the addition of dielectric nanostructures. Therefore, the system is idealized as a single plasmonic nanoparticle with radius equal to the effective radius of the system or a_{eff}. a_{eff} is calculated by

$$a_{eff} = \sqrt[3]{\frac{3V}{4\pi}}, \tag{2.1}$$

where V denotes the total volume of the system.

2.2. The Parameters of the Cancer Tissue

Cancer tissue has many different classifications, with the histological structures of the tissue changing dramatically. Cancer tissue is heterogeneous, with the tissue being composed of cancerous cells, healthy cells, and layers of adipose. A singular cell itself is also a heterogeneous structure, with changing optical properties in different organelles [87]. In this study, these impurities are ignored and a homogeneous medium is assumed for simplicity.

Since most cells are composed of approximately 70% water, most studies model human tissue as water [88]. As plasmonic absorption is dependent on the refractive index of the medium, the accuracy of the model can be improved by using accurate data. the refractive indexes of cancer tissue is dependent on the cancer type, because of the difference in cell structures in different parts of the body, resulting in different refractive indexes. The refractive indexes of some of the most common cancer types are presented in Table 2.1.

Table 2.1: Refractive indexes of cancer tissue in different places in the human body.

Type of Cancer	**Refractive Index**
Blood	1.390 [89, 90]
Breast	1.399 [89, 90]
Lung	1.370 [91]
Skin	1.380 [92]

Even though there are more than 100 types of cancer documented, breast and lung cancer cumulatively represents 24.7% of all new cases in 2021 with breast cancer being the most common with 284,200 new cases in the USA [93]. The medium in this study is modeled as a homogeneous volume with a refractive index of $m = 1.399 + i0$, as an approximation of breast cancer.

2.3. Nanoparticle Permeability of Cancer Tissue

Nanoparticles accumulate in the tumor tissue due to the EPR effect as briefly mentioned in Section 1.1. The general reasoning behind the EPR effect is the production of blood vessels for the exponential growth of the tumor cells. The abnormal structure of the vessels that form around the tumor has an increased permeability for nanostructures. The lack of effective lymphatic drainage in tumors allows for the increased retention of nanoparticles [94]. While the effectiveness of this phenomenon in human tissue has been in question in recent years [95], the EPR effect can be enhanced [96–98] and still is a crucial element of the applicability of PTT. Recent studies show that the EPR effect is dependent on the properties of the tumor itself, like intratumoral pressure and regional blood flow to the tumor [99]. This discovery results in a decrease in the cases treatable with PTT in which the EPR effect is solely responsible for nanoparticle distribution in the tumor tissue.

Because of the mechanisms behind the EPR effect, the permeability of the cancer tissue is dependent on the particle size and shape. Bawendi et al. [100] suggest cancer tissue has increased permeability for smaller nanoparticles, therefore allowing for a larger quantity of nanoparticles to be absorbed into the cancer tissue. This increased permeability also suggests that smaller nanoparticles are expelled from the cancer tissues quicker. Therefore, increasing the absorption of the smaller nanoparticles is crucial for the PTT to be most effective for maximum heating of the cancer tissue without the need for multiple doses, as the absorption of larger nanoparticles into the cancer tissue. The aforementioned study [100] also shows that cancer tissue has much lower permeability for nanoparticles larger than $125nm$ and lower retention for nanoparticles smaller than $10nm$.

In this study, the EPR effect will be used as a limiting factor for the sizes of both dielectric and metal nanoparticles. Smaller nanoparticles are prioritized for an increased number of nanoparticles in the cancer tissue. Usage of smaller nanoparticles allow for larger total volume of plasmonic nanoparticles to be introduced into the cancer tissue. And since the improvement method proposed in this thesis relies on the proximity of the plasmonic nanoparticles and the dielectric nanostructures, an increased number of nanoparticles is critical for the purposes of this study. For simplicity, the distribution of the nanoparticles inside the tumor tissue will also be defined as homogeneous, contrary to the heterogeneous distribution provided by EPR [101].

2.4. Toxicology of the Nanoparticles

Even though the different properties of nanoparticles compared to their bulk counterparts form the basis of nanotechnology, this discrepancy can also be the reason for some limitations in usage. For instance, Au, which in its bulk form is an inert metal, can show some toxicity for the human body in its nanoparticle state [102]. The large surface area-to-volume ratio of nanoparticles that allows them to be excellent scatterers and in some cases absorbers, also makes the nanoparticles chemically reactive [103]. This reactivity promotes the production of reactive oxygen species (ROS) in the tissue. The increased amount of ROS can result in inflammation in the cell, damage to the cellular proteins, and even damage to the DNA strands [104]. The controlled production of ROS is the main principle behind photodynamic therapy, referenced in Section 1.1 as in controlled dosages, the production of ROS can stimulate apoptosis in cells [105]. Nanotoxicity of nanoparticles is inversely related to nanoparticle size. Pan et al. found that nanoparticles that are $15nm$ in diameter show 60 times more toxicity compared to nanoparticles that are $1.4nm$ in diameter [106]. Nanoparticles also have different toxic effects on different cell types [107]. Some nanotoxicity data for commonly used nanoparticle materials is presented in Table 2.2.

Table 2.2: Nanotoxicological Effect of Most Commonly Used Nanoparticle Materials.

Nanoparticle Material	**Toxic Effects of Nanospheres**
Gold (Au)	Low to none immunotoxicity and genotoxicity induced in cell cultures [108]

Table 2.2. Nanotoxicological Effect of Most Commonly Used Nanoparticle Materials. (cont.)

Nanoparticle Material	**Toxic Effects of Nanospheres**
Silica (SiO_2)	SiO_2 nanoparticles show dose-dependent toxicity [109], an accumulation in lungs is expected [110]
Silicon (Si)	Si nanoparticles ($d = 5nm$) show toxicity in zebrafish embryo, similar results can be expected in human cells [111]
Silver (Ag)	Ag nanoparticles have toxicity in the form of ROS generation, and DNA damage *in vitro*, and show toxicity in the central nervous, circulatory, and respiratory systems *in vivo* [112]
Copper (Cu)	Cu nanoparticles of different sizes($40nm, 60nm, 80nm$) all induce severe toxicity in neurons *in vitro* [113]
Iron Oxide (Fe_3O_4)	Low to none immunotoxicity and genotoxicity induced in cell cultures [108]

Cytotoxicities of nanoparticles are not numerically represented, as the nanotoxicity is highly dependent on the size of the nanoparticles. Therefore, using nanotoxicity as a boundary condition for a simulation model is difficult. Nanotoxicity of the nanoparticles must be tested in cell cultures before their use in clinical studies. The experimental studies suggest the applicability of Au nanoparticles in human cases in controlled doses [114], whereas SiO_2 nanoparticles show mild toxicity *in vivo* [115].

2.5. Dipole Generation of Each Nanoparticle

In this study, the system of nanoparticle shapes considered are axisymmetric. The imperfect nature of a colloid system of nanoparticles cannot be precisely represented in this model. These nanoparticles are modeled as a set of infinitesimal points, or dipoles, for the purposes of simulating systems with different nanoparticle shapes. The simulation method used in the thesis, discrete dipole approximation, is explained in detail in Section 3.2. The dipole models of different nanoparticles used in this study is presented in Figure 2.4.

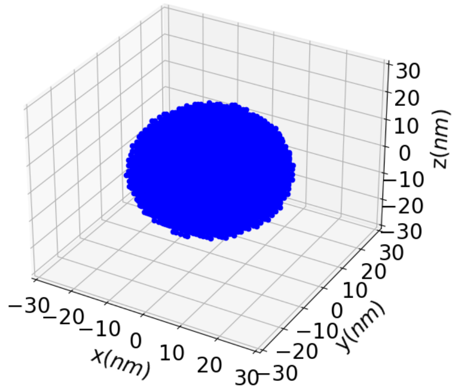

(a)

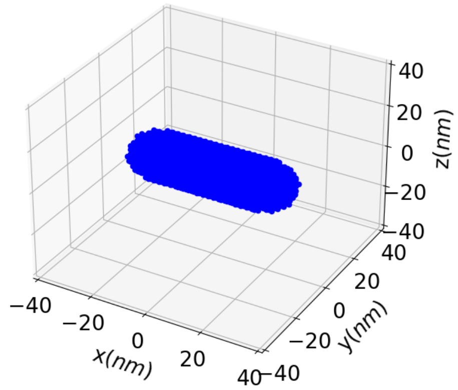

(b)

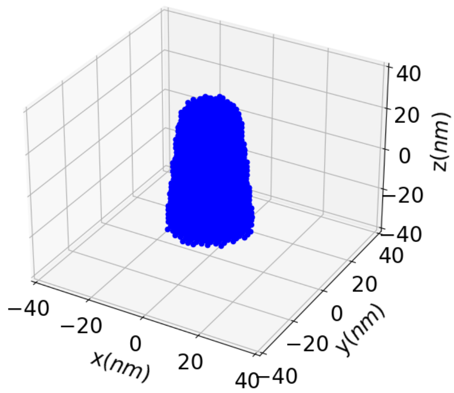

(c)

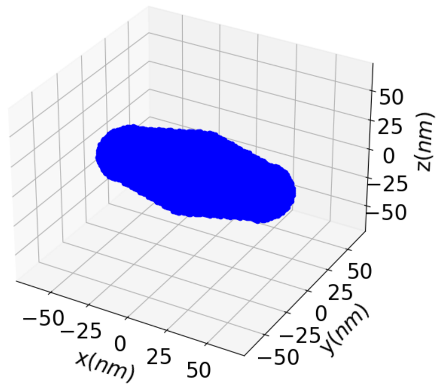

(d)

Figure 2.4: Dipoles of (a) a Nanosphere ($r_s = 10nm$), (b) a Nanorod ($r_r = 10nm, h_r = 60nm$), (c) a Nanocone ($r_{tip} = 10nm, h_c = 60nm, \beta = 10°$), (d) a Bipyramid Nanoparticle ($h_b = 120nm, r_b = 20nm, \beta = 30°$).

Each nanoparticle is separated into different heights denoted by z. A radius $r(z)$ is also defined around the z-axis. Each integer point (a, b, z) that lies on the xy-plane and is inside a circle with radius $r(z)$ is stored as per the requirements of the DDSCAT software used in the simulation. The calculation of dipole points in an arbitrary height

z is visualized in Figure 2.5. The $r(z)$ functions of different nanoparticles are given in Appendix A.

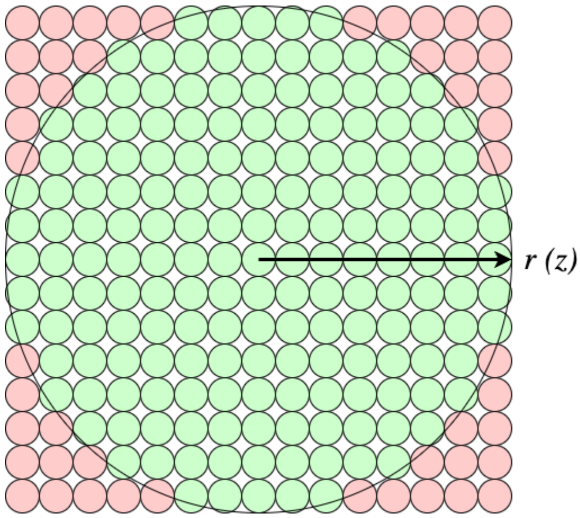

Figure 2.5: Dipoles Included in a Height z.

2.6. Cases Studied

The changes in absorption efficiency of the nanoparticles are studied by the changing of the parameters in different cases. The cases studied are limited by the computational time required for the simulations. Firstly, cases of prescribed nanoparticle placements are studied to understand which parameters of the probe effect the absorption efficiency. Then, these variables are changed in randomized placement cases. Any combined placements of the nanoparticles will be referred to as "systems" in this thesis. The absorption behaviour of these system are investigated based on absorption efficiency and cross section.

2.6.1. Single Plasmonic Nanosphere Case

The simplest case studied in the thesis is the light absorption of a single plasmonic nanosphere. The size of the nanoparticle is the only parameter changed to understand the effect of size on the absorption of a singular nanoparticle. Moreover, there is no need for orientational averaging, as the system is spherical.

2.6.2. Two Plasmonic Nanospheres Case

Two plasmonic nanoparticles are placed on the x-axis as shown in Figure 2.6. The distance between the two plasmonic nanospheres d_s, is kept constant as $20nm$.

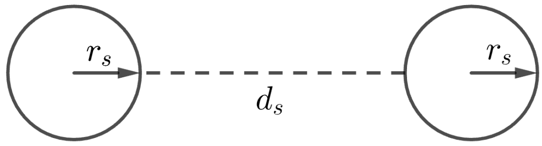

Figure 2.6: The Configuration of Two Plasmonic Nanospheres.

The nanospheres have radii of $r_{s,1}$ and $r_{s,2}$ respectively. The radii of the nanospheres are changed concurrently and separately. The absorption efficiency in the concurrent radius change case is compared to the results from the single plasmonic nanoparticle case, to understand the effect of plasmonic nanoparticles interacting with each other on the absorption efficiency. The absorption efficiency of the two nanoparticles with different radii is compared to another equivolumetric system composed of two plasmonic nanoparticles that have the same radius r_{eq} that is calculated by

$$r_{eq} = \sqrt[3]{\frac{r_{s,1}^3 + r_{s,2}^3}{2}}. \tag{2.2}$$

2.6.3. Two Plasmonic Nanoparticles - One Dielectric Probe Case

The objective of the study is to observe the behaviour of the plasmonic nanoparticles in close proximity with dielectric nanoparticles in a suspended environment. Since different shaped dielectric nanoparticles are considered, these cases are defined based on the shape of the dielectric nanoprobes. Nanospheres, nanorods, nanocones, and bipyramid nanoparticles are considered as the dielectric nanoprobes, to identify the effect of geometric parameters defining the nanoparticle shapes that on the absorption efficiency of the system as dielectric nanoprobes do not absorb light. For a more informing comparison in these cases, a modified definition of absorption Q'_{abs} is defined as

$$Q'_{abs} = \frac{C_{abs}}{\pi r_{plas}^2} = Q_{abs}(\frac{a_{eff}}{a_{plas}})^2, \tag{2.3}$$

where a_{plas} denotes the effective radius of the plasmonic nanoparticles.

2.6.3.1. Nanosphere Probe Case. This case is studied to understand the improvement of absorption with the addition of dielectric particles, even though a nanosphere is not an elongated particle. The radius of the dielectric nanosphere, $r_{s,d}$, is the only parameter changed. The configuration of the plasmonic nanoparticles and the dielectric nanosphere is given in Figure 2.7. The distance between the surface of the dielectric nanosphere and the middle of the two plasmonic nanoparticles d_p, is kept constant at $40nm$.

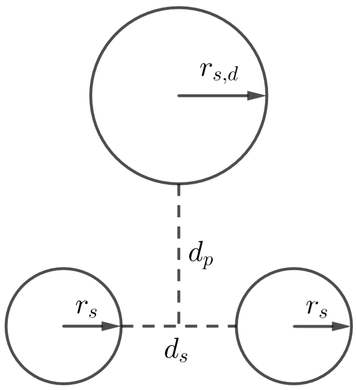

Figure 2.7: The Configuration of Nanosphere Case.

2.6.3.2. Nanorod Probe Case. A nanorod is considered next. Since a nanorod is an elongated shape, the improvement in absorption can be similar to the improvement from an AFM tip. The shape parameters of the nanorod; radius r_r and length h_r are changed and the effect on absorption is studied. The configuration of the plasmonic nanoparticles and the dielectric nanorod is given in Figure 2.8. The distance dielectric nanorod and the plasmonic nanoparticles d_p, is kept constant at $40nm$.

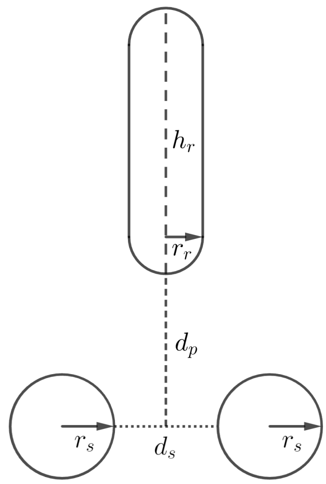

Figure 2.8: The Configuration of Nanorod Case.

2.6.3.3. Nanocone Case. Another nanoparticle considered is nanocone. The angled geometry of the nanocone more closely resembles an AFM tip, therefore being a suitable substitute. The shape parameters of the nanocone; radius r_c, length h_c, and tip angle β are changed and the effect on absorption is studied. The configuration of the plasmonic nanoparticles and the dielectric nanocone is given in Figure 2.9. The distance between the surface of the dielectric nanocone and the middle of the two plasmonic nanoparticles d_p, is kept constant at $40nm$.

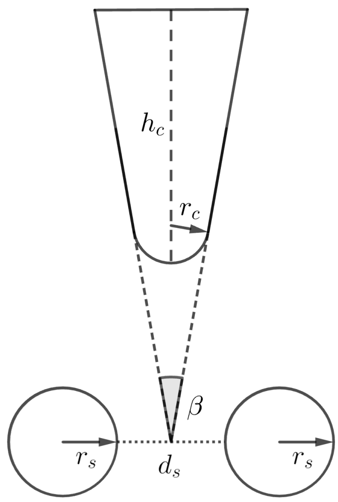

Figure 2.9: The Configuration of Nanocone Case.

<u>2.6.3.4. Bipyramid Nanoparticle Case.</u> Bipyramid nanoparticles are chosen as a probe shape because of the randomized orientation of the nanoparticles in PTT treatment. Since previous studies [77] suggest that the interaction between the tip of the probe and the plasmonic nanoparticle is the main reason behind the enhanced absorption, it is expected that using a nanoparticle with two tips will increase the average absorption efficiency. The shape parameters of the bipyramid nanoparticles; height h_b, and tip radius $r_{tip,b}$ are changed and the effect on absorption is studied. The configuration of the plasmonic nanoparticles and the dielectric bipyramid is given in Figure 2.10. The distance between the surface of the dielectric bipyramid and the middle of the two plasmonic nanoparticles d_p, is kept constant at $40nm$.

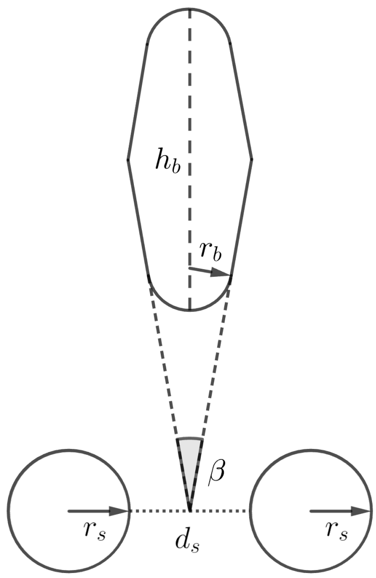

Figure 2.10: The Configuration of Bipyramid Nanoparticle Case.

2.6.4. Randomized Placement of Three Plasmonic Nanospheres - One Dielectric Nanostructure Case

The randomized systems are chosen to have a single probe and three plasmonic nanospheres. As SiO_2 has a higher toxicity compared to Au, a lower concentration of dielectric material is assumed. The optimal parameters of each probe shape are compared to understand which nanoparticle would be the most effective probe within the conditions set in Section 2.1. Examples of randomized placements are presented in Figure 2.11.

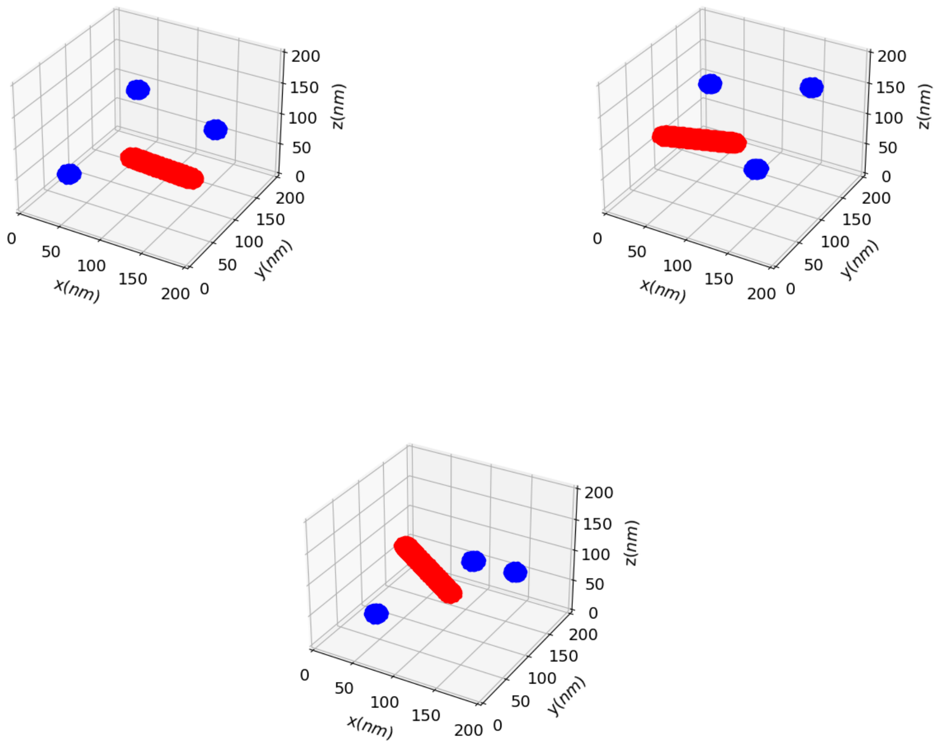

Figure 2.11: Placement Examples for Three Plasmonic Nanospheres ($r_s = 10nm$, shown in blue) and One Dielectric Nanorod ($r_r = 10nm, h_r = 100nm$, shown in red).

3. METHODOLOGY

3.1. Generalized Lorenz-Mie Theory

The Maxwell Equations is a set of partially differential equations which how the electric and magnetic fields behave and how these fields interact with each other [116]. These four equations form the base of optics. The solutions of these equations provide exact solutions to many electromagnetic phenomena. Mie Solution is a exact solution of the Maxwell Equations describing the behaviour of an incident linearly polarized wave by a homogeneous sphere suspended in a medium [117]. For incident beams that are circularly or elliptically polarized, the solution is called generalized Lorenz-Mie theory (GLMT). An open source MATLAB code for Mie Scattering and Absorption by Mätzler [118] is used in this study, since this package allows for anisotropic materials. While GLMT results are exact, the method has limitations regarding the geometry of the nanoparticle. GLMT does not apply to cases where scatterers are not spherical [117]. Therefore, GLMT is not applicable to this study and will only be used for verification purposes.

3.2. Discrete Dipole Approximation

Discrete dipole approximation (DDA) is a method of estimating the absorption and scattering characteristics of arbitrarily shaped particles first proposed by Purcell and Pennypacker in 1973 [119]. A larger object is approximately modeled as an array of much smaller polarizable spherical dipoles that are placed equidistantly with distance, d. The separation process for an arbitrarily shaped particle can be seen in Figure 3.1.

The interactions of the dipoles between each other and the incident field can be expressed as a set of linear equations, which can be solved to calculate individual dipole polarizations. Since the dipoles interact with each other by their electric fields, DDA is also sometimes referred to as coupled dipole approximation. From these polarizations, the scattering and the absorption of the system can be calculated. An open source implementation, referred as DDSCAT that was developed by Draine and Flatau [85]. In this study, DDSCAT is used for predicting the behaviour of nanoparticles.

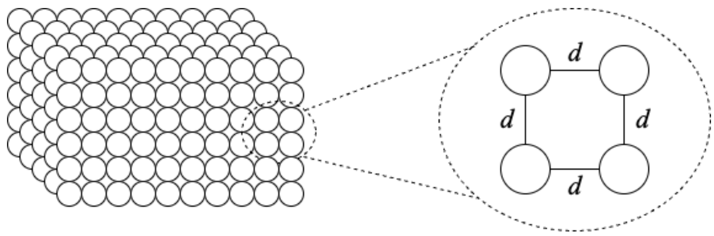

Figure 3.1: Rectangular Object Separated into Dipoles.

3.3. Comparison and Validation of Model

In order to show the validity of the models used in the study, the predictions of DDSCAT are compared to those of GLMT.

3.3.1. Single *Au* Nanosphere Results

A single Au nanosphere with a radius of $20nm$ is considered with a dipole spacing of $d = 1nm$. Q_{abs}, Q_{sca}, and Q_{ext} values are calculated for incident polarized radiation between 300 to $700nm$ in 20 uniformly distributed wavelengths. These efficiency (Q_i) results are related to cross-section (C_i) values by

$$C_i = Q_i \pi a_{eff}^2, \tag{3.1}$$

where i represents either "abs" for absorption, "sca" for scattering, or "ext" for extinction. Figure 3.2 shows the comparison between the C_{abs} values calculated by Mie theory and DDSCAT.

Figure 3.2 shows that the DDSCAT has a tendency to overestimate the absorption of the system in the $300-450nm$ range, but has excellent agreement in the LSPR range and beyond. This suggests that DDSCAT is well-suited for modeling Au nanospheres.

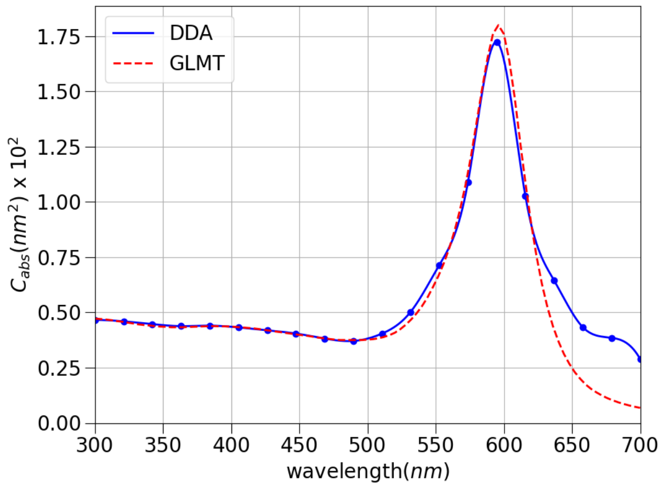

Figure 3.2: C_{abs} Comparison of a single Au nanosphere.

3.3.2. Single SiO_2/Au Core-Shell Nanoparticle Results

A single SiO_2/Au core-shell particle is considered next. The Au shell thickness is $10nm$, while the SiO_2 core radius is $20nm$.

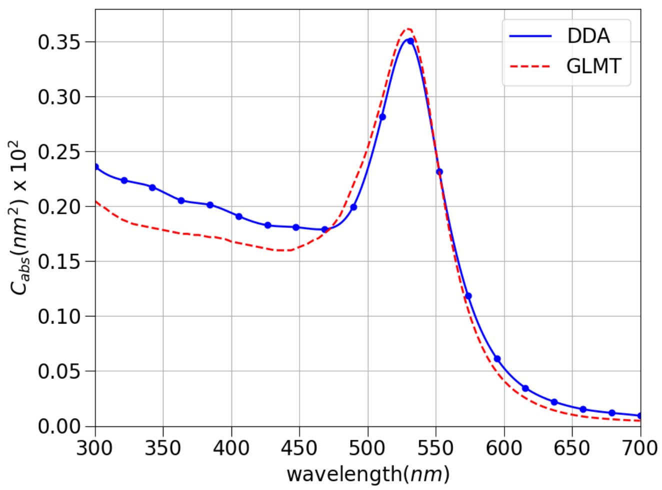

Figure 3.3: C_{abs} Comparison of a SiO_2/Au Core-Shell Nanoparticle.

Figure 3.3 shows that the DDSCAT model's agreement is excellent in the $300 - 600nm$ range. In larger wavelengths, the DDSCAT model overestimates the absorption cross-section of the system. Results in Figure 3.3 suggest that the model can be used to calculate the absorption of an Au and SiO_2 system.

3.3.3. Dipole Spacing

As previously mentioned in Section 2.5, the object interacting with the electromagnetic wave is discretized in terms of a finite number of dipoles in DDA. As the number of dipoles increases, the accuracy of the system also increases. However, the simulation time is also critical because of the randomized nature of the models studied in the thesis. The maximum dipole spacing d allowed in DDA is calculated by

$$|m|kd \leq 1, \tag{3.2}$$

where m denotes the complex refractive index of the target material, $k = 2\pi/\lambda$, and d denotes the interdipole spacing [85]. The maximum allowed interdipole spacings based on Equation 3.2 for the materials used in the thesis are given in Table 3.1.

Table 3.1: Maximum allowed interdipole spacing for the materials used in the thesis.

Target Material	**Maximum $\|m\|k$ Values**	**Maximum d Values (nm)**
Gold (Au)	58.6	17.0
Silica (SiO_2)	38.0	26.5

Since the DDA method simulates the coupled effects between dipole pairs, decreasing the number of dipoles greatly decreases the simulation time. The relation between the interdipole spacing and the number of dipoles can be approximated by

$$Vd^3 = N_{dipoles}, \tag{3.3}$$

where V denotes the total volume of the nanoparticles, N_{abs} denotes the number of dipoles, and d denotes the interdipole spacing. Using the relation in Equation (3.3) in

Equation (3.2) can be used as a criterion for the validity of the model. This equation is presented as

$$N_{dipoles} > (4\pi/3)|m|^3(ka_{eff})^3, \tag{3.4}$$

where a_{eff} denotes the effective radius, the radius of a sphere that is equivolumetric to the system.

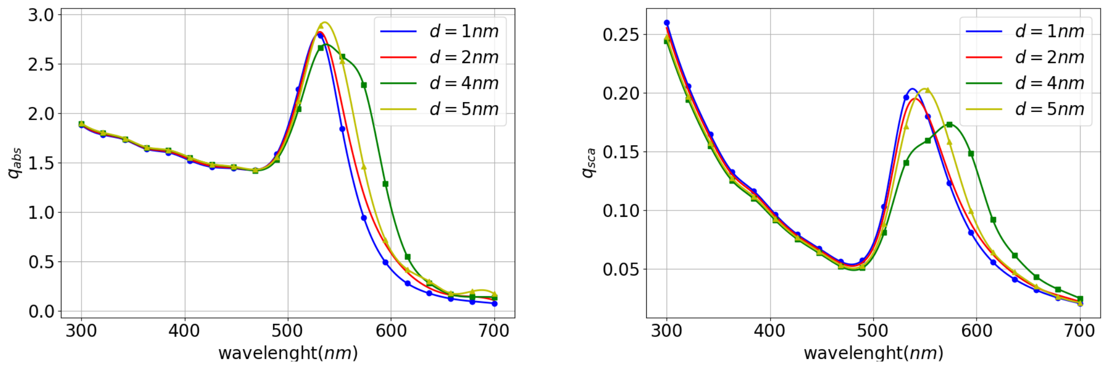

(a) (b)

Figure 3.4: Comparison of (a) Q_{abs} and (b) Q_{sca} for a Single Au Nanosphere ($r = 20nm$) with Changing Interdipole Spacing d.

$d = 1nm$ can be assumed to be an exact result because of the compatibility of results seen in Figure 3.2. From Figure 3.4, it can be observed that solutions with $d = 2nm$ is independent from total dipole number used as these solutions yield near identical results with those of $d = 1nm$. Table 3.2 shows Q_{abs} values and the simulation time for each dipole spacing.

Table 3.2: Simulation times and the LSPR peaks of different interdipole spacings in modeling a single Au nanosphere ($r = 20nm$).

Interdipole Spacing(d)	**Number of Dipoles($\mathbf{N_{abs}}$)**	**Simulation Time(s)**	**LSPR Peak(nm)**	$\mathbf{Q_{abs,LSPR}}$
1 nm	33400	37840.83	532	2.79
2 nm	4168	8233.71	532	2.83
4 nm	514	1648.32	541	2.67
5 nm	256	1022.59	540	2.91

The results presented in Table 3.2 show that the decrease in the simulation time is significant when d is increased. A redshift in the LSPR peak is observed in larger dipole spacings. The accuracy of the Q_{abs} calculations also decrease with larger d values. Therefore, $d = 2nm$ is chosen to decrease the calculation time while having acceptable accuracy.

4. RESULTS AND DISCUSSION

4.1. Single Plasmonic Nanosphere

The effect of size on the absorption of light by plasmonic nanoparticles are well documented. But preliminary simulations are carried out to see the effect of changing the size of nanoparticles in a medium like breast cancer tissue. The results are shown in Figure 4.1.

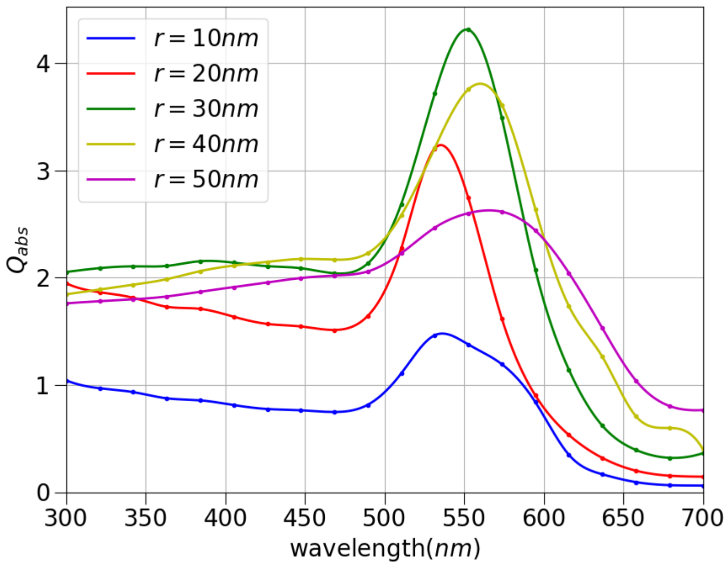

Figure 4.1: Q_{abs} of Single Au Nanosphere with Changing Radius r_s.

The data presented in Figure 4.1 is consistent with the results seen in literature [120–122]. Redshift in the LSPR peaks, and an increase in Q_{abs} until a threshold where scattering becomes the main mode of extinction can both be observed as the nanoparticle size increases. However, the definition of Q_{abs} should also be taken into consideration. Considering that the major objective of the study is to increase the absorbed energy, change in C_{abs} should also be considered, that is also related to the absorbed energy. Since the size of the nanoparticle affects the number of nanoparticles in the cancer tissue in PTT, the volume of the nanoparticle must also be considered when comparing the absorbing properties of nanoparticles. Therefore, it can be argued

$$C'_{abs} = \frac{C_{abs}}{\pi a_{eff}^3} = \frac{Q_{abs}}{\pi a_{eff}}, \tag{4.1}$$

is another important parameter to comment on for this case, since C'_{abs} shows the absorption effectiveness of each nanoparticle. Q'_{abs} of different nanosphere sizes are shown in Figure 4.2.

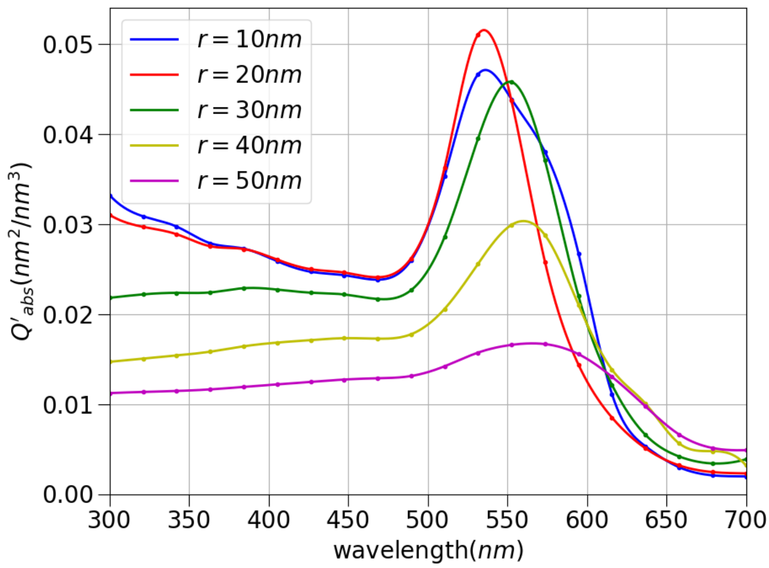

Figure 4.2: Q'_{abs} of Single Au Nanosphere with Changing Radius r.

Figure 4.2 shows that smaller nanoparticles absorb more light in relation to their volume, which means that in total a large number of small nanoparticles absorb more incident light compared to a small number of large nanoparticles. This can be attributed to the fact that smaller nanoparticles have a larger percentage of their atoms in the surface region, having enhanced surface plasmons as a result. These results in conjunction with the improved permeability of smaller nanoparticles in cancer tissues suggest that smaller nanoparticles are more suitable for PTT applications.

4.2. Two Plasmonic Nanospheres

4.2.1. Changing the Plasmonic Nanosphere Sizes Concurrently

In many applications, including PTT, plasmonic particles at various concentrations are utilized. Considering such cases, it is important to understand the absorption enhancement resulting from interparticle coupling effects. Figure 4.3 shows Q_{abs} values of two plasmonic nanospheres with changing r.

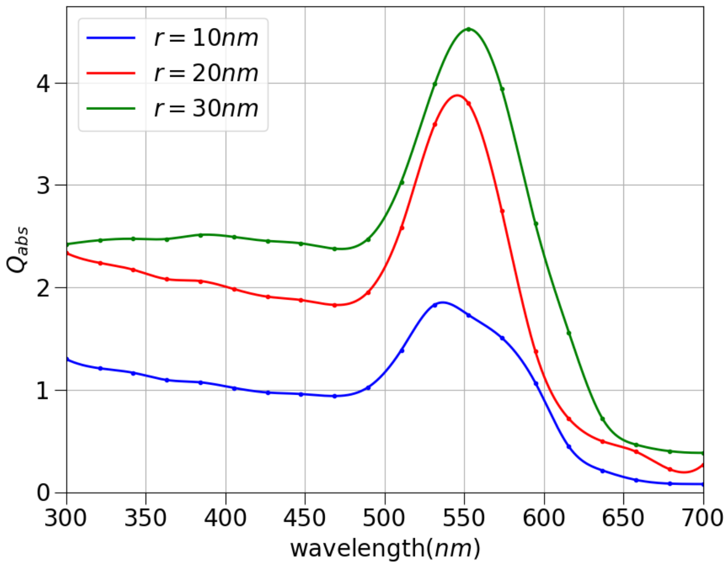

Figure 4.3: Q_{abs} of Two Au Nanospheres with Changing Radii r.

Similar to the results in Section 4.1, larger nanoparticles have higher Q_{abs} values. In the case where there are no interparticle coupling effects, it can be assumed that Q_{abs} of the system remains constant. To understand the effect of the proximity of the two plasmonic nanoparticles on absorption efficiency, the results shown in Figure 4.3 is compared to the single plasmonic nanoparticle case in Section 4.1. The Q_{abs} values for a single plasmonic nanoparticle are referred to as $Q_{abs,0}$. The $Q_{abs}/Q_{abs,0}$ results are presented in Figure 4.4. An improvement can be observed in all cases. When the incident light has a shorter wavelength than the LSPR wavelength, a consistent improvement at a rate of 1.2 can be observed. The stability of the $r_s = 10nm$ results can be attributed to the distance between the nanospheres. The distance between the nanoparticles with respect to their sizes is much larger when compared to $r_s = 20nm$ and $r_s = 30nm$. Therefore, the coupling effect between the nanoparticles are weaker compared to the larger particles, making the improvement much more consistent as it is mostly reliant on the scattering of light by one particle onto the other. The fluctuations seen in Figure 4.4 for $r_s = 20nm$ and $r_s = 30nm$ are the result of more pronounced coupling effects between the nanoparticles because of the relative proximity of these nanospheres with respect to their sizes as the coupling effects of nanoparticles is related to the incident wavelength.

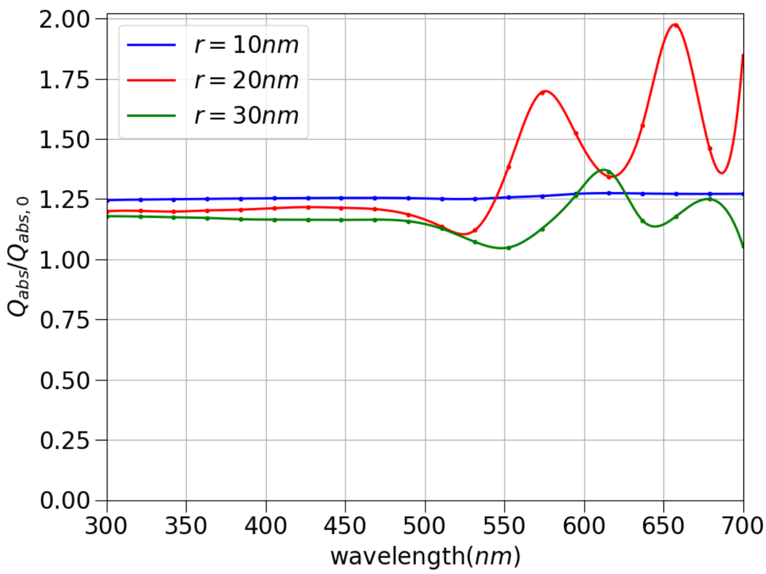

Figure 4.4: $Q_{abs}/Q_{abs,0}$ of Two Au Nanospheres with Changing Radii r_s.

4.2.2. Changing the Plasmonic Nanosphere Sizes Separately

The Q_{abs} values of systems of two plasmonic nanoparticles with different sizes are compared to equivolumetric systems of two nanoparticles with same size to understand if a size difference between the plasmonic nanoparticles has any effect on the interparticle coupling effects. The radii of the plasmonic nanoparticles in the equivolumetric system is calculated by Equation 2.2. The results are given in Figure 4.5.

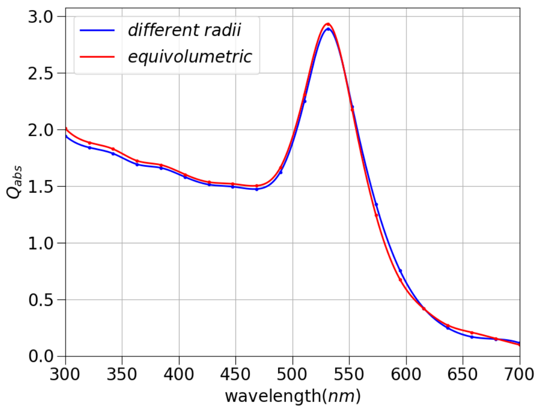

(a)

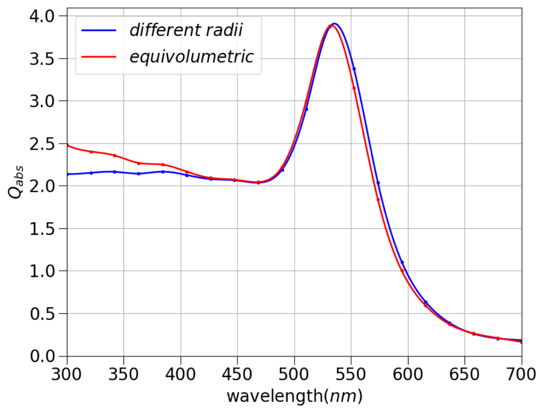

(b)

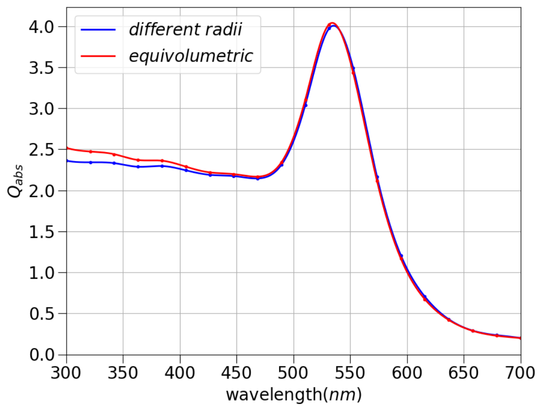

(c)

Figure 4.5: Q_{abs} of Two Au Nanospheres with Different Radii and the Equivolumetric System (a) $r_1 = 10nm, r_2 = 20nm$, (b) $r_1 = 10nm, r_2 = 30nm$, and (c) $r_1 = 20nm, r_2 = 30nm$.

Figure 4.5 shows that the Q_{abs} results stay relatively constant. This result can be attributed to the fact that the different sizes of the nanoparticles all have the same order of magnitude, and therefore have similar optical properties. More drastic changes in the nanoparticle sizes can yield other results, but since nanoparticles larger than $r = 30nm$ might not be suitable for PTT applications, simulations of larger nanospheres are deemed unnecessary.

4.3. Two Plasmonic Nanospheres with One Dielectric Nanoparticle

As explained in Section 2.6.3, the main focus of this study is to understand the behaviour of plasmonic nanoparticles when in close proximity with dielectric nanoparticles. The following simulations are preliminary research and are executed to understand which parameters of the dielectric nanoparticle will have a positive impact on the absorption efficiency of the system. Therefore, the parameters of the plasmonic nanoparticles will not be changed following this section. The radius of the nanosphere r_s, the distance between the spheres d_s, and the quantity of the spheres will be kept constant at $10nm$, $20nm$, and 2, respectively. The reasoning behind choosing $r_s = 10nm$ even though $r_s = 20nm$ demonstrates better optical properties is the maximization of enhancement by the addition of the dielectric nanostructure and the increased permeability of the cancer tissue for smaller nanoparticles. The effects of the increased concentration are explained in Section 4.1. In earlier studies found in the literature on the increase in absorption by the addition of dielectric probes, the AFM probe is relatively infinite in length compared to the plasmonic nanoparticles as mentioned in Section 1.4.2.3. While the sizes of the studied dielectric nanostructures will not reach relative infinity and will be limited to $125nm$, it can be assumed that a significant size difference between the plasmonic nanosphere and the dielectric nanostructure is needed for the dielectric nanostructure to have a positive impact on total absorption.

4.3.1. Nanosphere Case

The first dielectric particle studied is the nanosphere, as the addition of a dielectric particle can promote some enhancement in the absorption. The optical interactions between a dielectric nanosphere and a plasmonic nanosphere with regards to the absorption enhancement promoted by the addition of the dielectric nanosphere are not studied extensively. Figure 4.6 shows the Q'_{abs} of the system when the radius of the dielectric nanosphere $r_{s,d}$ is changed. A system without any dielectric particle will be referred to as the "base system" and will be presented for comparison in this and all following figures.

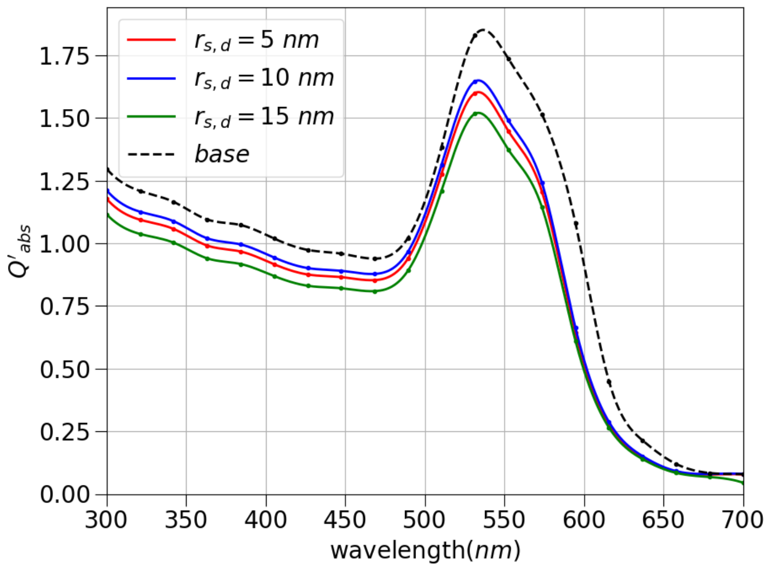

Figure 4.6: Q'_{abs} of a System with SiO_2 Nanosphere with Changing Probe Radius $r_{s,d}$.

Figure 4.6 shows that the addition of the spherical nanosphere is not an effective method of improving the absorption of the plasmonic nanospheres. Table 4.1 shows the maximum Q_{abs} and Q'_{abs} values for changing r_s values.

Table 4.1: Effects of changing the radius of dielectric nanosphere, r_s on absorption.

$\mathbf{r_s}(nm)$	$\mathbf{a_{eff}}(nm)$	$\mathbf{Q_{abs}}$	$\mathbf{Q'_{abs}}$
base	12.6	1.852	1.852
5 nm	12.9	1.530	1.683
10 nm	14.4	1.263	1.650
15 nm	17.5	0.788	1.521

Table 4.1 shows that the addition of the dielectric nanosphere diminishes both the absorption efficiency and the total absorption of the system. This decrease can be attributed to the increased scattering area as the dielectric nanostructure scatters away more of the incident light. The results show that the addition of nanosphere probes does not improve any desirable properties in the system. Therefore, dielectric nanospheres as a method for enhancing total absorption will not be considered further.

4.3.2. Nanorod Case

Nanorods are the second type of dielectric nanostructure studied, due to their simple and elongated geometry. The effects of tip radius, r_r, and nanorod length, h_r, are studied in order to understand their effect on the absorption efficiency.

4.3.2.1. Changing the Length h_r of the Nanorod. Figure 4.7 shows the Q'_{abs} of the system when the radius of the probe h_r is changed. The tip radius, r_r, of the nanorod is kept constant at $10nm$.

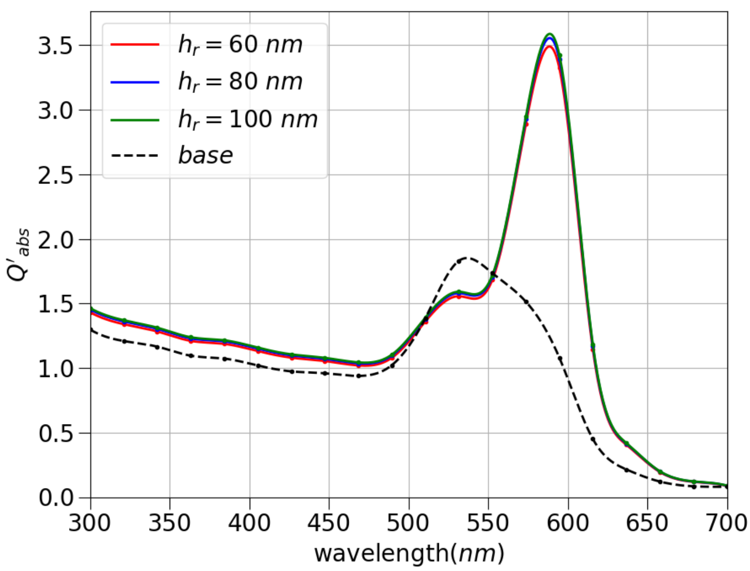

Figure 4.7: Q'_{abs} of a System with SiO_2 Nanorod with Changing Rod Length h_r.

A drastic improvement in Q'_{abs} can be observed with the addition of dielectric nanorod. A significant redshift in the LSPR peak is also observed following the introduction of the dielectric nanorod. The wider range of the LSPR peak mentioned in Section 4.1 can be defined as a proclivity towards a redshift. Table 4.2 shows the maximum Q_{abs} and Q'_{abs} values for changing h_r values.

Table 4.2: Effects of changing the length of dielectric nanorod, h_r on absorption.

$\mathbf{h_r}(nm)$	$\mathbf{a_{eff}}(nm)$	$\mathbf{Q_{abs}}$	$\mathbf{Q'_{abs}}$
base	12.6	1.852	1.852
60 nm	18.2	1.673	3.491
80 nm	19.6	1.469	3.556
100 nm	20.8	1.317	3.588

It can be observed in Table 4.2 that while Q'_{abs} increases slightly as h_r increases, there is no pronounced relationship between the length of the probe h_r and Q'_{abs}. In contrast an inverse relationship between h_r and Q_{abs} can be observed, which can be used to comment on how effective the addition of dielectric material is. This is contradictory to the expectation of increased electric field enhancement as the dielectric nanostructure size reaches relative infinity compared to the Au nanosphere. Therefore, it can be assumed that 0-D nanorods enhance the absorption by nanoparticles in lengths much smaller than what could be defined as relative infinity, since their increased length does not promote additional absorption in a meaningful manner. However, a drastic increase in Q'_{abs} is observed when the dielectric nanostructure is introduced. Therefore, it can be stated that the use of dielectric nanorods with plasmonic nanoparticles can be beneficial in increasing absorption when the system can be controlled.

<u>4.3.2.2. Changing the Radius r_r of the Nanorod.</u> Figure 4.8 shows the Q'_{abs} of the system when the radius of the probe r_r is changed. The nanorod length, h_r, of the nanorod is kept constant at $60nm$.

The redshift in Figure 4.7 can also be observed in Figure 4.8. It is important to note that the LSPR wavelength is not affected by changes in either h_r or r_r. Therefore, it can be assumed that the redshift is not related to the properties of the nanorod, but to the presence of the dielectric nanostructure. Table 4.3 shows shows the maximum Q_{abs} and Q'_{abs} values for changing r_r values.

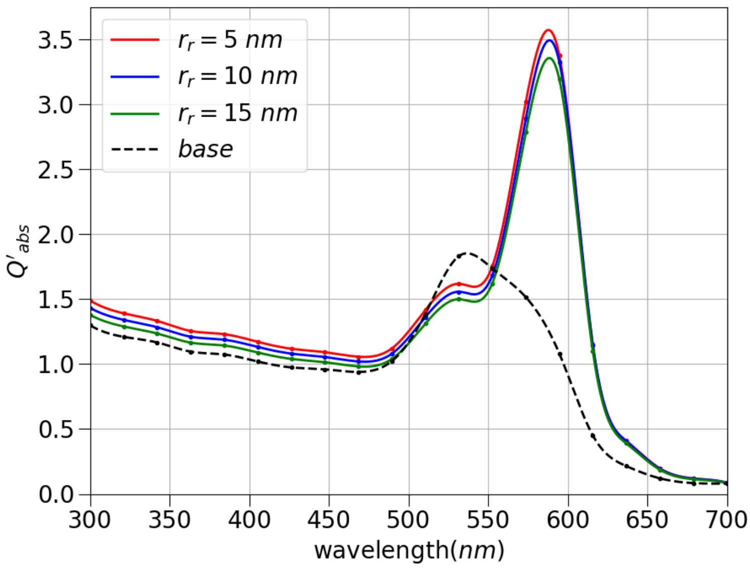

Figure 4.8: Q'_{abs} of a System with SiO_2 Nanorod with Changing Rod Radius r_r.

A comparison of the probe systems shows that r_r and Q'_{abs} also have an inverse relationship. $r_r = 5nm$ has the highest absorption efficiency Q'_{abs}, with an increase of 81.6% compared to the base system at its LSPR peak. This enhancement also demonstrates that the Q_{abs} of the system can also be enhanced by the addition of 0-D dielectric nanoparticles.

Table 4.3: Effects of changing the radius of dielectric nanorod, r_r on absorption.

$\mathbf{r_r}(nm)$	$\mathbf{a_{eff}}(nm)$	$\mathbf{Q_{abs}}$	$\mathbf{Q'_{abs}}$
base	12.6	1.852	1.852
5 nm	16.5	2.082	3.570
10 nm	18.2	1.673	3.491
15 nm	21.8	1.121	3.354

4.3.3. Nanocone Case

Nanocones are one of the most promising nanostructure types in this study, because of their close resemblance to an AFM probe, as mentioned in Section 2.6.3.3. Each parameter of the nanocone is studied in this section to understand the optimal properties of a nanocone for absorption enhancement.

4.3.3.1. Changing the Length h_c of the Nanocone. Figure 4.9 shows the Q'_{abs} of the system with changing nanocone length, h_c. Tip angle, β, and tip radius, r_{tip}, are kept constant at 10° and $10nm$ respectively.

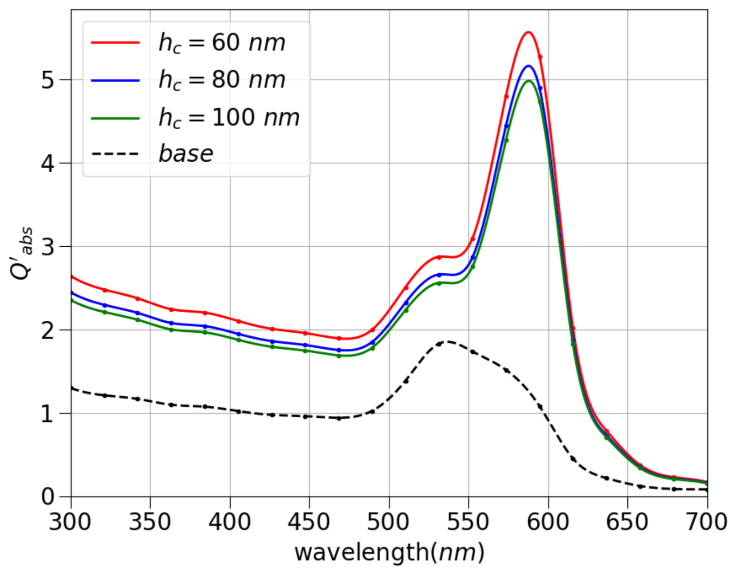

Figure 4.9: Q'_{abs} of a System with SiO_2 Nanocone with Changing Probe Length h_c.

Similar to the findings in Section 4.3.2, a redshift in the LSPR peak is observed. Figure 4.9 also shows a negative correlation between h_c and Q'_{abs}. While unexpected because of the results in Section 4.3.2, this phenomenon increases the applicability of these dielectric nanoparticle - plasmonic nanoparticle mixtures in PTT. Table 4.4 shows shows the maximum Q_{abs} and Q'_{abs} values for changing h_c values.

Table 4.4: Effects of changing the length of dielectric nanocone, h_c on absorption.

$\mathbf{h_c}(nm)$	$\mathbf{a_{eff}}(nm)$	$\mathbf{Q_{abs}}$	$\mathbf{Q'_{abs}}$
base	12.6	1.852	1.852
60 nm	20.8	2.044	5.570
80 nm	22.1	1.673	5.165
100 nm	23.4	1.445	4.985

4.3.3.2. Changing the Tip Radius r_{tip} of the Nanocone. Figure 4.10 shows the Q_{abs} of the system when the length of the probe, h_c, is changed. Tip angle β and probe length h_c are constant at 10° and 60nm respectively.

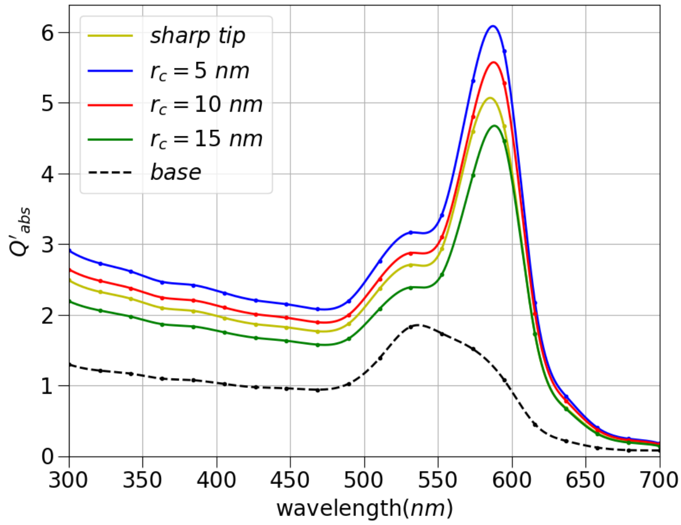

Figure 4.10: Q'_{abs} of a System with SiO_2 Nanocone with Changing Tip Radius r_{tip}.

Figure 4.10 shows an inverse relation between r_c and Q'_{abs} for spherical tips. These simulations show that nanocones that have sharper tips, tend to be better suited for absorption improvement. A similar phenomenon can be observed in conductors in the macroscale, where a stronger electric field is observed around sharper tips since a larger electrical charge is focused in a smaller volume, creating a stronger electric field around the tip. But, it can be seen that $r_c = 5nm$ nanocone system has a higher Q'_{abs} peak compared to the sharp-tipped nanocone system. Therefore, it can be assumed that spherical tipped nanocones are better enhancers. This phenomenon can be explained by the definition of a sharp tip. Since all electric fields must be perpendicular to the surface, a spherical tip must exist. The definition of a sharp tipped nanocone is therefore intrinsically incorrect, as r_c can never be 0. Table 4.5 shows shows the maximum Q_{abs} and Q'_{abs} values for changing r_c values.

Table 4.5: Effects of changing the tip radius of dielectric nanocone, r_c on absorption.

$\mathbf{r_c}(nm)$	$\mathbf{a_{eff}}(nm)$	$\mathbf{Q_{abs}}$	$\mathbf{Q'_{abs}}$
base	12.6	1.852	1.852
sharp tip	15.4	2.657	5.067
5 nm	18.6	2.791	6.083
10 nm	20.8	2.044	5.570
15 nm	23.4	1.492	4.672

4.3.3.3. Changing the Tip Angle β of the Nanocone. Figure 4.11 shows the Q'_{abs} of the system when the length of the probe β is changed. Tip radius, r_{tip}, and probe length, h_c, are kept constant at $10nm$ and $60nm$ respectively.

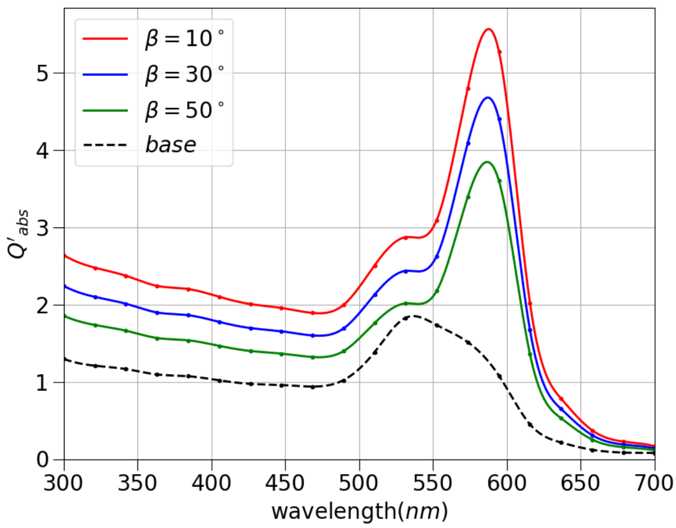

Figure 4.11: Q'_{abs} of a System with SiO_2 Nanocone with Changing Probe Tip Angle β.

Figure 4.11 shows that lower β volumes should be preferred. This result is consistent with previous findings as increasing tip angle, β, decreases the sharpness of the tip. Another side effect of the increased β is the increased surface area of the nanocone, increasing the scattering area.

Table 4.6: Effects of changing the tip angle of dielectric nanocone, β on absorption.

β	$\mathbf{a_{eff}}\,(nm)$	$\mathbf{Q_{abs}}$	$\mathbf{Q'_{abs}}$
base	12.6	1.852	1.852
10°	20.8	2.044	5.570
30°	24.6	1.228	4.682
50°	28.9	0.779	4.099

Table 4.6 shows shows the maximum Q_{abs} and Q'_{abs} values for changing β values. A drastic decrease in both Q_{abs} and Q'_{abs} is observed when β increases. These findings are compliant with the results in Section 4.3.3.2 as sharper tips enhance the electric field near the tip region more effectively.

4.3.4. Bipyramid Nanoparticle Case

Bipyramid nanoparticles are modeled as two joint nanocones. Therefore, some insight from Section 4.3.3 can be applied here. The most important point is the size of the nanocone that is pointing towards the nanoparticles. The effect of tip angle β is not studied, since changes in β do not affect the probe geometry any differently compared to nanocones. β is also taken to be constant at 10°.

4.3.4.1. Changing the Length h_b of the Bipyramid Nanoparticle. Figure 4.12 shows the Q'_{abs} of the system when the length of the probe, h_c, is changed. Tip radius, $r_{tip,b}$, of the bipyramid nanoparticle is taken to be $10nm$.

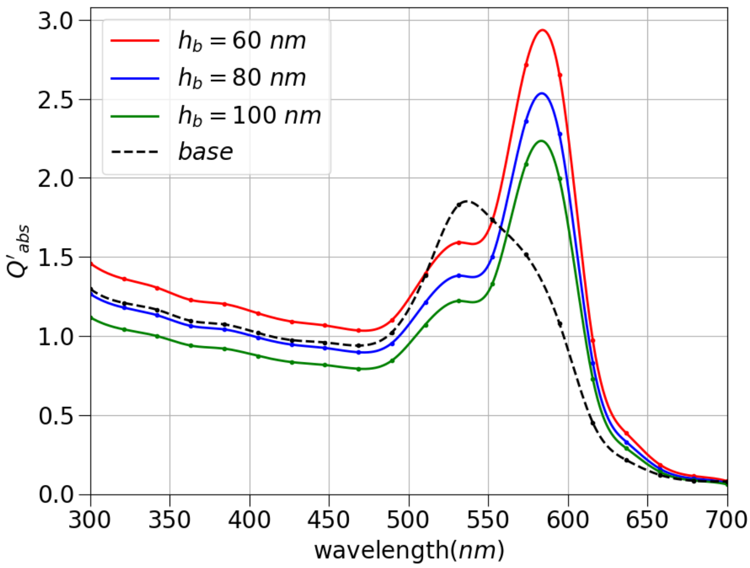

Figure 4.12: Q'_{abs} of a System with SiO_2 Bipyramid Nanoparticle with Changing Bipyramid Nanoparticle Length h_b.

While the system exhibits similar behavior to the previous systems presented in Sections 4.3.3 and 4.3.2 such as the redshift in the LSPR peak, comparisons between the nanocone cases and the nanorod cases show that the improvements from the bipyramids are comparable to nanorods. Table 4.7 shows the maximum Q_{abs} and Q'_{abs} values for changing h_b values.

Table 4.7: Effects of changing the length of dielectric bipyramid nanoparticle, h_b on absorption.

$\mathbf{h_b}$**(nm)**	$\mathbf{a_{eff}}$**(nm)**	$\mathbf{Q_{abs}}$	$\mathbf{Q'_{abs}}$
base	12.6	1.852	1.852
60 nm	19.2	1.264	2.936
80 nm	20.7	0.939	2.535
100 nm	21.9	0.739	2.234

Table 4.7 shows that Q_{abs} and Q'_{abs} of the system decreases when h_b increases, but an overall increase in absorption is seen compared to the base system.

4.3.4.2. Changing the Tip Radius $r_{tip,b}$ of the Bipyramid Nanoparticle. Figure 4.13 shows the Q'_{abs} of the system when the tip radius of the probe, $r_{tip,b}$, is changed. h_c of the bipyramid nanoparticle is taken to be $60nm$.

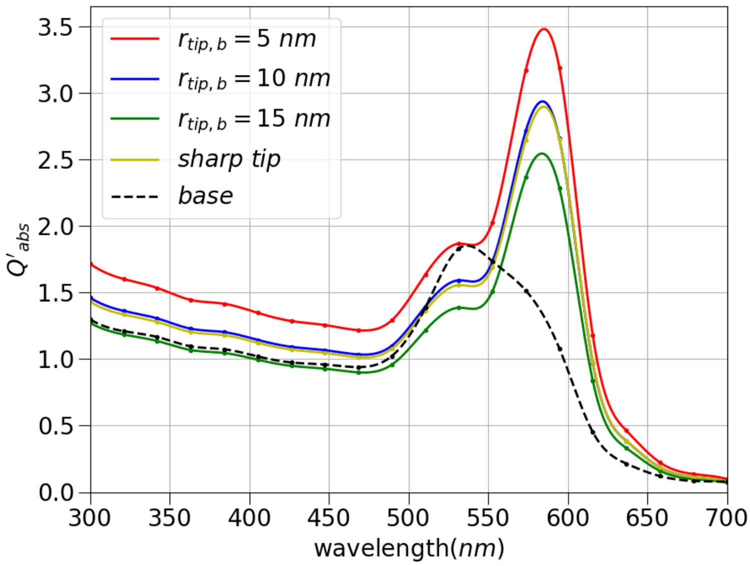

Figure 4.13: Q'_{abs} of a System with SiO_2 Bipyramid Nanoparticle with Changing Bipyramid Tip Radius $r_{tip,b}$.

The bipyramid nanoparticle exhibits similar properties to the nanocone studied in Section 4.3.3; an increase in absorption is seen when tip radius is smaller. These results are expected, as the tip section of the bipyramid nanoparticle that is near the plasmonic nanoparticles has the same geometry with the nanocone. Table 4.8 shows the maximum Q_{abs} and Q'_{abs} values for changing $r_{tip,b}$ values.

Table 4.8: Effects of changing the tip radius of dielectric bipyramid nanoparticle, $r_{tip,b}$ on absorption.

$\mathbf{r_{tip,b}}$**(nm)**	$\mathbf{a_{eff}}$**(nm)**	$\mathbf{Q_{abs}}$	$\mathbf{Q'_{abs}}$
base	12.6	1.852	1.852
sharp tip	14.9	2.071	2.896
5 *nm*	16.3	2.105	3.522
10 *nm*	19.2	1.264	2.881
15 *nm*	21.3	0.890	2.552

Comparison between the nanocone and bipyramid nanoparticle shows that the enhancement of electric field by the nanocone is better than the bipyramid nanoparticle, with a 71.9% difference in Q'_{abs}, and a 32.6% difference in Q_{abs} when both the dielectric nanoparticles are in their optimal states. Therefore, it could be argued that the upper half of the nanocone is crucial for enhanced electric field around the tip. Since there are two points for the electric field to be focused around, the electric field enhancement around the plasmonic nanospheres by the dielectric nanoparticle is effectively halved.

4.4. Randomized Placement of Three Plasmonic Nanospheres - Single Dielectric Nanostructure Case

In Section 4.3, different types of nanoparticles were proposed as probes to understand which parameters of each particle is important to enhance the absorption efficiency of the systems. The highest amount of improvement from each type of nanoparticle structure observed in Sections 4.3.2, 4.3.3, and 4.3.4 are presented in Figure 4.14.

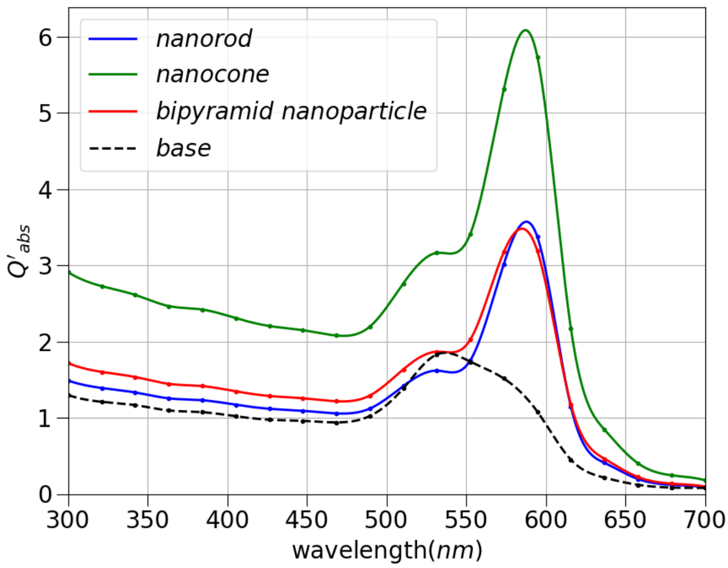

Figure 4.14: Q'_{abs} of a System with Two Au Nanospheres and Single SiO_2 Nanostructure in Prescribed Positions, Nanocone ($r_c = 5nm, h_c = 60nm, \beta = 10°$), Nanorod ($r_r = 5nm, h_r = 60nm$), Bipyramid Nanoparticle ($r_b = 5nm, h_c = 60nm, \beta = 10°$).

Figure 4.14 suggest that nanocone is the best candidate for PTT applications if the placements of the nanoparticles can be controlled, with a 228.5% increase in Q'_{abs}. But, because of the delivery method of nanoparticles into the cancer tissue, the orientations of the nanoparticles cannot be controlled. Therefore, the results presented in Figure 4.14 can only be taken as a road-map. For applicability in PTT, randomized orientations must be simulated. Since the interactions between nanoparticles is reliant on the placements, a single case must be simulated many times. Figure 4.15 shows the absorption efficiency of the randomized system that includes three plasmonic nanoparticles and one dielectric probe.

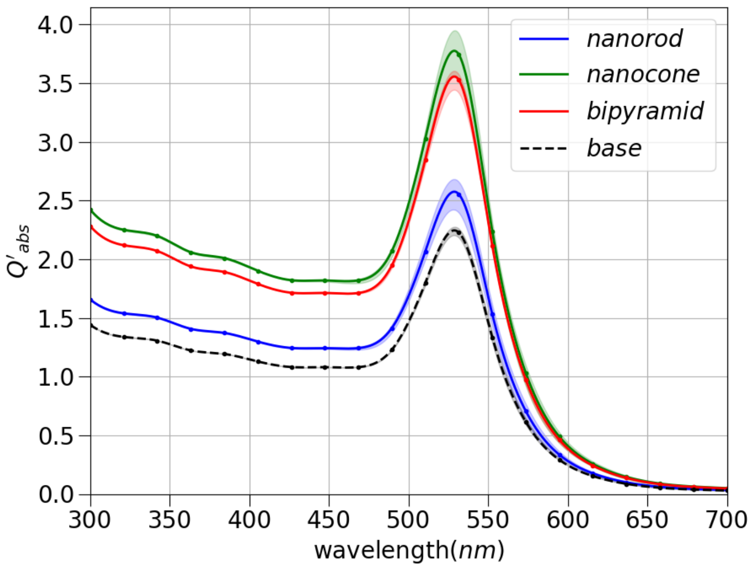

Figure 4.15: Averaged Q'_{abs} ($average\ \pm 5\%$) of a System with Three Au Nanospheres and One SiO_2 Probe in Randomized Positions; Nanocone ($r_{tip} = 5nm, h_c = 60nm, \beta = 10°$), Nanorod ($r_r = 5nm, h_r = 60nm$), Bipyramid Nanoparticle ($Sharp\ Tip, h_c = 60nm, \beta = 10°$).

It can be seen that introduction of nanocones and bipyramid nanoparticles in randomized orientations and positions generally improve the absorption efficiency of the plasmonic nanoparticles with nanocones being the most effective probe, improving the absorption efficiency of the system by 68.1%. The bipyramid nanoparticles produce similar results, with an improvement of 58.3%. The similar enhancements of bipyramid nanoparticles and nanocones, especially when compared to the difference in Figure 4.14 show that the concept of a symmetric nanoparticle with multiple tips is more effective compared to an asymmetric nanoparticle with a single tip region. Since the enhancement of electric fields occur around the tip of the dielectric nanoparticles, positive effects can only be observed when the tip of the nanoparticle is positioned towards the plasmonic nanoparticles. With bipyramids, the probability of a tip region pointing towards the plasmonic nanoparticles is doubled compared to the nanocones.

The addition of nanorods to randomized a randomized system resulted in a small increase in absorption of 5.29%. Comparison between bipyramid nanoparticles and nanorods shows that the slanted nature of nanocones is crucial for absorption enhancement in randomized placements since the enhancement of these particles was similar in Figure 4.14. These results show that slanted nanoparticles are more effective probes, both in prescribed and randomized positioning cases.

The redshift seen in Sections 4.3.2, 4.3.3, and 4.3.4 is not observed in Figure 4.15 since the occurrence of the redshift is dependent on both the existence of the probe and the distance between the nanoparticles.

The relationship between the Q'_{abs} values and the energy absorbed over time by the systems can be calculated by combining Equations (3.1), (1.2) and (2.3) into

$$\frac{\Phi_{e,abs,probe}}{\Phi_{e,abs,no\ probe}} = \frac{Q_{abs,probe}a^2_{eff,probe}}{Q_{abs,no\ probe}a^2_{eff,no\ probe}} = \frac{Q'_{abs,probe}}{Q'_{abs,no\ probe}}. \tag{4.2}$$

The percentage improvement of adding dielectric probes into the system is presented in Table 4.9.

Table 4.9: Average improvement of energy absorbed by the addition of probes.

Probe	$\mathbf{a_{eff}}$**(nm)**	$\mathbf{Q'_{abs}}$	**Improvement(percentage)**
None	14.4	2.246	-
Cone	17.8	3.775	68.1%
Rod	16.1	2.365	5.3%
Bipyramid	17.6	3.556	58.3%

Table 4.9 suggests that the addition of material is a larger contributor to higher levels of absorption in systems, as even nanorod systems demonstrate higher total absorption compared to the base systems. It can also be observed that the volume of the added probe is more effective in increasing the total absorption. However, the total

mass of the dielectric or metal nanoparticles cannot be increased indiscriminately. The toxicological effects presented in Section 2.4 are results seen *in vivo*, but the long-term effects of nanoparticles in human tissue is not well documented.

5. CONCLUSION

This thesis aimed to increase the absorption efficiency of plasmonic nanoparticles by adding a dielectric nanoparticle, in photothermal therapy applications. Plasmonic and dielectric nanoparticles are first studied in controlled placements to better understand how different geometric parameters affect the total absorption of the system. Then, optimal cases for different dielectric structures are randomly placed along with three plasmonic nanoparticles in a control volume. For simplicity, the distribution of the nanoparticles in the control volume was assumed to be homogeneous. The nanoparticles were also assumed to be stationary in the cancer tissue. Discrete dipole approximation is used in the study to accurately model the randomized placements of nanoparticles with different compositions and shapes. Current research on absorption behaviour with the addition of a dielectric substance is still mostly focuses on controlled environments, as nanotechnology is still far from having widespread use in society. But, having a better understanding of the thermo-optical properties of nanoparticles in uncontrollable environments is a crucial step in nanotechnological advancements.

In both prescribed and randomized placements, a noticeable improvement in absorption efficiency based on the volume of plasmonic nanoparticles in the system was observed in almost all cases. Surprisingly, it was generally observed that absorption of the system has a inverse relationship with the size of the dielectric nanoparticle. However, it was observed that an elongated geometry is critical for the dielectric nanostructure to be beneficial for the system. Comparison between types of dielectric nanoparticles showed that while these nanoparticles must have two different dimensions, the size differences between the plasmonic nanoparticles and the probes do not need to be as large as once assumed. Therefore, it could be inferred that the smallest sizes of these dielectric nanoparticles were enough to enhance the electric field in the tip region, and larger dielectric nanoparticles only increased the total scattered light. The comparison between the nanorods and nanocones also showed the crucial role of slope in the dielectric nanostructure for better electric field improvement around the tip region of the dielectric nanostructure.

The main point of further improvement in this thesis is the more accurate modeling of randomized placement in PTT, and further independence studies. In the current state of the thesis, a predefined number of nanoparticles are simply placed around centers in the control volume separately and assumed to be stationary in these points. A more realistic model would have the placements and movements of the nanoparticles dependant on many factors, like the formation of aggregates because of opposite surface charges. The effect of the plasmonic nanoparticle number on the improved absorption is also not studied. An independence study on the number of plasmonic nanoparticles is needed to better understand the effectiveness of the dielectric nanostructure. In the current state of the thesis, it is not known whether the improvements observed are a function of the number of plasmonic nanoparticles, or the result of the addition of the dielectric nanostructures into the system. One of the main assumptions in defining the control volume is the safety gap. While the $\frac{3r_s}{2}$ distance is taken from existing literature, and is accepted to be the limit where plasmonic nanoparticles are not affecting each other, the enhancement or diminishing of absorption by the addition of the dielectric nanostructures at larger distances is not studied.

Any enhancement presented in this thesis is derived only from the interactions between a dielectric nanoparticle and the plasmonic nanoparticles. In most studies involving AFM probes as a method for improving the absorption efficiency of plasmonic nanoparticles, the plasmonic nanoparticles are placed upon a surface. These surfaces can be approximated by the addition of laminas into the dielectric nanoparticle-plasmonic nanoparticle mixture. Laminas, which are rod-like nanoparticles that have a $d/h < 50$, can be used as surface areas for the plasmonic nanoparticles to be close to. While it is difficult for the plasmonic nanoparticles to be placed in a controlled manner on the laminas, a flat surface near the plasmonic nanoparticles in a randomized system can have a positive impact on the absorption of the system. Another method of improvement is the reduction of randomization. Magnetic core - dielectric shell nanorods can be used as the dielectric nanoparticles introduced to the system. And with the introduction of a magnetic field to the system, the orientations of the probes can be controlled. Another method of reducing the effect of randomization can be the usage of nanostars. A larger number of tips can allow for a more consistent improvement in absorption efficiency.

Photothermal therapy is a bleeding-edge treatment method for cancer. But most research on photothermal therapy focuses on improving with the addition of a secondary treatment method. By increasing the efficiency of absorption, the irradiation time or the irradiation dose can be decreased, therefore improving both the effectiveness of treatment and life quality. But the application area of these results can be more encompassing. By manipulating the thermo-optical properties of randomly scattered nanoparticles, the manufacturing cost of many inventions like transparent solar cells can be greatly decreased. Therefore, I believe the study I have concluded can be a good first step into meaningful research.

REFERENCES

1. Jemal, A., R. Siegel, E. Ward, Y. Hao, J. Xu and M. J. Thun, "Cancer Statistics, 2009", *CA: A Cancer Journal for Clinicians*, Vol. 59, No. 4, pp. 225–249, 2009.

2. Zugazagoitia, J., C. Guedes, S. Ponce, I. Ferrer, S. Molina-Pinelo and L. Paz-Ares, "Current challenges in cancer treatment", *Clinical Therapeutics*, Vol. 38, No. 7, pp. 1551–1566, 2016.

3. Fisher, B., "Biological and clinical considerations regarding the use of surgery and chemotherapy in the treatment of primary breast cancer", *Cancer*, Vol. 40, No. S1, pp. 574–587, 1977.

4. Schirrmacher, V., "From chemotherapy to biological therapy: A review of novel concepts to reduce the side effects of systemic cancer treatment", *International Journal of Oncology*, Vol. 54, No. 2, pp. 407–419, 2019.

5. Love, R. R., H. Leventhal, D. V. Easterling and D. R. Nerenz, "Side effects and emotional distress during cancer chemotherapy", *Cancer*, Vol. 63, No. 3, pp. 604–612, 1989.

6. Nurgali, K., R. T. Jagoe and R. Abalo, "Adverse effects of cancer chemotherapy: Anything new to improve tolerance and reduce sequelae?", *Frontiers in Pharmacology*, Vol. 9, 2018.

7. Saito, A. M., M. B. Landrum, B. A. Neville, J. Z. Ayanian and C. C. Earle, "The effect on survival of continuing chemotherapy to near death", *BMC Palliative Care*, Vol. 10, No. 1, pp. 1–11, 2011.

8. Krause, S., J. Debus and D. Neuhof, "Radiotherapy", *Recent results in cancer research. Fortschritte der Krebsforschung. Progrès dans les recherches sur le cancer*, Vol. 183, pp. 285–91, 2011.

9. Barazzuol, L., R. P. Coppes and P. van Luijk, "Prevention and treatment of radiotherapy-induced side effects", *Molecular Oncology*, Vol. 14, No. 7, pp. 1538–1554, 2020.

10. Mohan, G., A. H. T.P., J. A.J., A. N. Saradha Devi K.M. and B. Vellingiri, "Recent advances in radiotherapy and its associated side effects in cancer—a review", *The Journal of Basic and Applied Zoology*, Vol. 80, No. 1, pp. 1–10, 2019.

11. Iyer, A. K., G. Khaled, J. Fang and H. Maeda, "Exploiting the enhanced permeability and retention effect for tumor targeting", *Drug Discovery Today*, Vol. 11, No. 17-18, pp. 812–818, 2006.

12. Kobayashi, H., R. Watanabe and P. L. Choyke, "Improving conventional enhanced permeability and retention (EPR) effects; what is the appropriate target?", *Theranostics*, Vol. 4, No. 1, p. 81, 2014.

13. Singh, R. and J. W. Lillard Jr, "Nanoparticle-based targeted drug delivery", *Experimental and Molecular Pathology*, Vol. 86, No. 3, pp. 215–223, 2009.

14. Kumari, P., B. Ghosh and S. Biswas, "Nanocarriers for cancer-targeted drug delivery", *Journal of Drug Targeting*, Vol. 24, No. 3, pp. 179–191, 2016.

15. Kwatra, D., A. Venugopal and S. Anant, "Nanoparticles in radiation therapy: a summary of various approaches to enhance radiosensitization in cancer", *Translational Cancer Research*, Vol. 2, No. 4, pp. 330–342, 2013.

16. Dougherty, T. J., C. J. Gomer, B. W. Henderson, G. Jori, D. Kessel, M. Korbelik, J. Moan and Q. Peng, "Photodynamic Therapy", *JNCI: Journal of the National Cancer Institute*, Vol. 90, No. 12, pp. 889–905, 1998.

17. Shang, L., X. Zhou, J. Zhang, Y. Shi and L. Zhong, "Metal Nanoparticles for Photodynamic Therapy: A Potential Treatment for Breast Cancer", *Molecules*,

Vol. 26, No. 21, 2021.

18. Park, W., Y.-J. Heo and D. K. Han, "New opportunities for nanoparticles in cancer immunotherapy", *Biomaterials Research*, Vol. 22, No. 1, pp. 1–10, 2018.

19. Yetisgin, A. A., S. Cetinel, M. Zuvin, A. Kosar and O. Kutlu, "Therapeutic nanoparticles and their targeted delivery applications", *Molecules*, Vol. 25, No. 9, p. 2193, 2020.

20. Liu, Y., P. Bhattarai, Z. Dai and X. Chen, "Photothermal therapy and photoacoustic imaging via nanotheranostics in fighting cancer", *Chemical Society Reviews*, Vol. 48, No. 7, pp. 2053–2108, 2019.

21. Zhi, D., T. Yang, J. O'hagan, S. Zhang and R. F. Donnelly, "Photothermal therapy", *Journal of Controlled Release*, Vol. 325, pp. 52–71, 2020.

22. Huang, X., P. K. Jain, I. H. El-Sayed and M. A. El-Sayed, "Plasmonic photothermal therapy (PPTT) using gold nanoparticles", *Lasers in Medical Science*, Vol. 23, No. 3, pp. 217–228, 2008.

23. Estelrich, J. and M. A. Busquets, "Iron oxide nanoparticles in photothermal therapy", *Molecules*, Vol. 23, No. 7, p. 1567, 2018.

24. Zhang, Y., X. Zhan, J. Xiong, S. Peng *et al.*, "Temperature-dependent cell death patterns induced by functionalized gold nanoparticle photothermal therapy in melanoma cells", *Scientific Reports*, Vol. 8, No. 1, pp. 1–9, 2018.

25. Syntichaki, P. and N. Tavernarakis, "Death by necrosis. Uncontrollable catastrophe, or is there order behind the chaos?", *EMBO Reports*, Vol. 3, No. 7, pp. 604–609, 2002.

26. Elmore, S., "Apoptosis: a review of programmed cell death", *Toxicologic Pathology*, Vol. 35, No. 4, pp. 495–516, 2007.

27. Sheng, Z., D. Hu, M. Xue, M. He, P. Gong and L. Cai, “Indocyanine green nanoparticles for theranostic applications”, *Nano-Micro Letters*, Vol. 5, No. 3, pp. 145–150, 2013.

28. Yoon, H.-J., H.-S. Lee, J.-Y. Lim and J.-H. Park, “Liposomal indocyanine green for enhanced photothermal therapy”, *ACS Applied Materials & Interfaces*, Vol. 9, No. 7, pp. 5683–5691, 2017.

29. Liu, S., X. Pan and H. Liu, “Two-dimensional nanomaterials for photothermal therapy”, *Angewandte Chemie International Edition*, Vol. 132, No. 15, pp. 5943–5953, 2020.

30. Huang, X., I. H. El-Sayed, W. Qian and M. A. El-Sayed, “Cancer cell imaging and photothermal therapy in the near-infrared region by using gold nanorods”, *Journal of the American Chemical Society*, Vol. 128, No. 6, pp. 2115–2120, 2006.

31. Feynman, R. P., “There’s Plenty of Room at the Bottom : An Invitation to Enter a New Field of Physics”, *Engineering and Science*, Vol. 23, pp. 22–36, 1960.

32. Taniguchi, N., *On the Basic Concept of ’Nano-Technology’*, 1974.

33. Drexler, K. E., *Engines of Creation: The Coming Era of Nanotechnology*, Anchor Press, Doubleday, 1986.

34. Karmakar, S., S. Kumar, R. Rinaldi and G. Maruccio, “Nano-electronics and spintronics with nanoparticles”, *Journal of Physics: Conference Series*, Vol. 292, p. 012002, IOP Publishing, 2011.

35. Homberger, M. and U. Simon, “On the application potential of gold nanoparticles in nanoelectronics and biomedicine”, *Philosophical Transactions of the Royal Society A: Mathematical, Physical and Engineering Sciences*, Vol. 368, No. 1915, pp. 1405–1453, 2010.

36. Parthasarathi, V. and G. Thilagavathi, "Synthesis and characterization of zinc oxide nanopartilce and its application on fabrics for microbe resistant defence clothing", *International Journal of Pharmacy and Pharmaceutical Sciences*, Vol. 3, No. 4, pp. 392–398, 2011.

37. Mokkapati, S., F. Beck, A. Polman and K. Catchpole, "Designing periodic arrays of metal nanoparticles for light-trapping applications in solar cells", *Applied Physics Letters*, Vol. 95, No. 5, p. 053115, 2009.

38. Suliman, A. E., Y. Tang and L. Xu, "Preparation of ZnO nanoparticles and nanosheets and their application to dye-sensitized solar cells", *Solar Energy Materials and Solar Cells*, Vol. 91, No. 18, pp. 1658–1662, 2007.

39. Temple, T. and D. Bagnall, "Optical properties of gold and aluminium nanoparticles for silicon solar cell applications", *Journal of Applied Physics*, Vol. 109, No. 8, p. 084343, 2011.

40. McNamara, K. and S. A. Tofail, "Nanoparticles in biomedical applications", *Advances in Physics: X*, Vol. 2, No. 1, pp. 54–88, 2017.

41. Saallah, S. and I. W. Lenggoro, "Nanoparticles carrying biological molecules: Recent advances and applications", *KONA Powder and Particle Journal*, Vol. 35, pp. 89–111, 2018.

42. Saleh, T. A. and V. K. Gupta, "Synthesis, classification, and properties of nanomaterials", *Nanomaterial and Polymer Membranes*, pp. 83–133, Elsevier, 2016.

43. Khlebtsov, N. G. and L. A. Dykman, "Optical properties and biomedical applications of plasmonic nanoparticles", *Journal of Quantitative Spectroscopy and Radiative Transfer*, Vol. 111, No. 1, pp. 1–35, 2010.

44. Pal, S. L., U. Jana, P. K. Manna, G. P. Mohanta and R. Manavalan, "Nanoparticle: An overview of preparation and characterization", *Journal of Applied Phar-*

maceutical Science, Vol. 1, pp. 228–234, 2011.

45. Yadav, T. P., R. M. Yadav and D. P. Singh, "Mechanical milling: a top down approach for the synthesis of nanomaterials and nanocomposites", *Nanoscience and Nanotechnology*, Vol. 2, No. 3, pp. 22–48, 2012.

46. Parashar, M., V. K. Shukla and R. Singh, "Metal oxides nanoparticles via sol–gel method: a review on synthesis, characterization and applications", *Journal of Materials Science: Materials in Electronics*, Vol. 31, No. 5, pp. 3729–3749, 2020.

47. Link, S. and M. A. El-Sayed, "Size and temperature dependence of the plasmon absorption of colloidal gold nanoparticles", *The Journal of Physical Chemistry B*, Vol. 103, No. 21, pp. 4212–4217, 1999.

48. Pareek, V., A. Bhargava, R. Gupta, N. Jain and J. Panwar, "Synthesis and Applications of Noble Metal Nanoparticles: A Review", *Advanced Science, Engineering and Medicine*, Vol. 9, pp. 527–544, 2017.

49. Rai, M., A. P. Ingle, S. Birla, A. Yadav and C. A. D. Santos, "Strategic role of selected noble metal nanoparticles in medicine", *Critical Reviews in Microbiology*, Vol. 42, No. 5, pp. 696–719, 2016.

50. Yang, Y., M. Zhang, H. Song and C. Yu, "Silica-Based Nanoparticles for Biomedical Applications: From Nanocarriers to Biomodulators", *Accounts of Chemical Research*, Vol. 53, No. 8, pp. 1545–1556, 2020.

51. Decker, M. and I. Staude, "Resonant dielectric nanostructures: a low-loss platform for functional nanophotonics", *Journal of Optics*, Vol. 18, No. 10, p. 103001, 2016.

52. Chavali, M. S. and M. P. Nikolova, "Metal oxide nanoparticles and their applications in nanotechnology", *SN Applied Sciences*, Vol. 1, No. 6, p. 607, 2019.

53. Zhang, Y., D. Petibone, Y. Xu, M. Mahmood, A. Karmakar, D. Casciano, S. Ali

and A. S. Biris, “Toxicity and efficacy of carbon nanotubes and graphene: the utility of carbon-based nanoparticles in nanomedicine”, *Drug Metabolism Reviews*, Vol. 46, No. 2, pp. 232–246, 2014.

54. Neelgund, G. M. and A. Oki, “Advancement in Photothermal Effect of Carbon Nanotubes by Grafting of Poly(amidoamine) and Deposition of CdS Nanocrystallites”, *Industrial & Engineering Chemistry Research*, Vol. 57, No. 23, pp. 7826–7833, 2018.

55. Romero, G. and S. E. Moya, *Chapter 4 - Synthesis of Organic Nanoparticles*, Vol. 4 of *Frontiers of Nanoscience*, pp. 115–141, Elsevier, 2012.

56. Chatterjee, K., S. Sarkar, K. J. Rao and S. Paria, “Core/shell nanoparticles in biomedical applications”, *Advances in Colloid and Interface Science*, Vol. 209, pp. 8–39, 2014.

57. Ghosh Chaudhuri, R. and S. Paria, “Core/shell nanoparticles: classes, properties, synthesis mechanisms, characterization, and applications”, *Chemical Reviews*, Vol. 112, No. 4, pp. 2373–2433, 2012.

58. Chen, H., L. Shao, Q. Li and J. Wang, “Gold nanorods and their plasmonic properties”, *Chemical Society Reviews*, Vol. 42, No. 7, pp. 2679–2724, 2013.

59. Pérez-Juste, J., I. Pastoriza-Santos, L. M. Liz-Marzán and P. Mulvaney, “Gold nanorods: synthesis, characterization and applications”, *Coordination Chemistry Reviews*, Vol. 249, No. 17-18, pp. 1870–1901, 2005.

60. Oh, N., B. H. Kim, S.-Y. Cho, S. Nam, S. P. Rogers, Y. Jiang, J. C. Flanagan, Y. Zhai, J.-H. Kim, J. Lee *et al.*, “Double-heterojunction nanorod light-responsive LEDs for display applications”, *Science*, Vol. 355, No. 6325, pp. 616–619, 2017.

61. Hsu, C.-M., C. Battaglia, C. Pahud, Z. Ruan, F.-J. Haug, S. Fan, C. Ballif and Y. Cui, “High-efficiency amorphous silicon solar cell on a periodic nanocone back

reflector", *Advanced Energy Materials*, Vol. 2, No. 6, pp. 628–633, 2012.

62. Ximen, H. and P. E. Russell, "Microfabrication of AFM tips using focused ion and electron beam techniques", *Ultramicroscopy*, Vol. 42, pp. 1526–1532, 1992.

63. Zheng, P., S. Kasani and N. Wu, "Converting plasmonic light scattering to confined light absorption and creating plexcitons by coupling a gold nano-pyramid array onto a silica–gold film", *Nanoscale Horizons*, Vol. 4, No. 2, pp. 516–525, 2019.

64. Weng, G., X. Shen, J. Li, J. Zhu, J. Yang and J. Zhao, "Multipole plasmon resonance in gold nanobipyramid: Effects of tip shape and size", *Physics Letters A*, Vol. 412, p. 127577, 2021.

65. Huang, X., P. Jain, I. El-Sayed and M. El-Sayed, "Gold nanoparticles: interesting optical properties and recent applications in cancer diagnostics and therapy. Nanomedi-cine 2 (5), 681–693 (2007)", *Proceedings of the International Conference on Production Engineering*, 2007.

66. Pilot, R., R. Signorini, C. Durante, L. Orian, M. Bhamidipati and L. Fabris, "A review on surface-enhanced Raman scattering", *Biosensors*, Vol. 9, No. 2, p. 57, 2019.

67. Miles, R. B., W. R. Lempert and J. N. Forkey, "Laser rayleigh scattering", *Measurement Science and Technology*, Vol. 12, No. 5, p. R33, 2001.

68. Khlebtsov, N. G., "Anisotropic properties of plasmonic nanoparticles: depolarized light scattering, dichroism, and birefringence", *Journal of Nanophotonics*, Vol. 4, No. 1, p. 041587, 2010.

69. Lang, X., L. Qian, P. Guan, J. Zi and M. Chen, "Localized surface plasmon resonance of nanoporous gold", *Applied Physics Letters*, Vol. 98, No. 9, p. 093701, 2011.

70. Mayer, K. M. and J. H. Hafner, “Localized surface plasmon resonance sensors”, *Chemical Reviews*, Vol. 111, No. 6, pp. 3828–3857, 2011.

71. Cao, C. and S. J. Sim, “Resonant Rayleigh light scattering response of individual Au nanoparticles to antigen–antibody interaction”, *Lab on a Chip*, Vol. 9, No. 13, pp. 1836–1839, 2009.

72. Petryayeva, E. and U. J. Krull, “Localized surface plasmon resonance: Nanostructures, bioassays and biosensing—A review”, *Analytica Chimica Acta*, Vol. 706, No. 1, pp. 8–24, 2011.

73. Link, S. and M. A. El-Sayed, “Size and temperature dependence of the plasmon absorption of colloidal gold nanoparticles”, *The Journal of Physical Chemistry B*, Vol. 103, No. 21, pp. 4212–4217, 1999.

74. Olson, J., S. Dominguez-Medina, A. Hoggard, L.-Y. Wang, W.-S. Chang and S. Link, “Optical characterization of single plasmonic nanoparticles”, *Chemical Society Reviews*, Vol. 44, No. 1, pp. 40–57, 2015.

75. Yu, P., Y. Yao, J. Wu, X. Niu, A. L. Rogach and Z. Wang, “Effects of plasmonic metal core-dielectric shell nanoparticles on the broadband light absorption enhancement in thin film solar cells”, *Scientific Reports*, Vol. 7, No. 1, pp. 1–10, 2017.

76. Rugar, D. and P. Hansma, “Atomic force microscopy”, *Physics Today*, Vol. 43, No. 10, pp. 23–30, 1990.

77. Huda, G. M. and J. T. Hastings, “Absorption Modulation of Plasmon Resonant Nanoparticles in the Presence of an AFM Tip”, *IEEE Journal of Selected Topics in Quantum Electronics*, Vol. 19, No. 3, pp. 4602306–4602306, 2013.

78. Talebi Moghaddam, S., H. Ertürk and M. P. Mengüç, “Enhancing local absorption within a gold nano-sphere on a dielectric surface under an AFM probe”, *Journal*

of Quantitative Spectroscopy and Radiative Transfer, Vol. 178, pp. 124–133, 2016.

79. Talebi Moghaddam, S., D. Avşar, H. Ertürk and M. Pınar Mengüç, "Effect of the probe location on the absorption by an array of gold nano-particles on a dielectric surface", *Journal of Quantitative Spectroscopy and Radiative Transfer*, Vol. 197, pp. 106–113, 2017.

80. Avşar, D., H. Ertürk and M. P. Mengüç, "Absorption and plasmon resonance of Bi-metallic core-shell nanoparticles on a dielectric substrate near an external tip", *Journal of Quantitative Spectroscopy and Radiative Transfer*, Vol. 241, p. 106684, 2020.

81. Aspnes, D. E. and A. A. Studna, "Dielectric functions and optical parameters of Si, Ge, GaP, GaAs, GaSb, InP, InAs, and InSb from 1.5 to 6.0 eV", *Physical Review B*, Vol. 27, pp. 985–1009, 1983.

82. Malitson, I. H., "Interspecimen Comparison of the Refractive Index of Fused Silica∗,†", *Journal of the Optical Society of America*, Vol. 55, No. 10, pp. 1205–1209, 1965.

83. Philipp, H. R., "Optical Properties of Silicon Nitride", *Journal of The Electrochemical Society*, Vol. 120, No. 2, p. 295, 1973.

84. Johnson, P. B. and R. W. Christy, "Optical Constants of the Noble Metals", *Physical Review B*, Vol. 6, pp. 4370–4379, 1972.

85. Draine, B. T. and P. J. Flatau, "User Guide for the Discrete Dipole Approximation Code DDSCAT 7.3", *Proceedings of the International Conference on Production Engineering*, 2013.

86. Ivezić, Z. and M. P. Mengüç, "An investigation of dependent/independent scattering regimes using a discrete dipole approximation", *International Journal of Heat and Mass Transfer*, Vol. 39, No. 4, pp. 811–822, 1996.

87. Liu, P., L. K. Chin, W. Ser, H. Chen, C.-M. Hsieh, C.-H. Lee, K.-B. Sung, T. Ayi, P. Yap, B. Liedberg, K. Wang, T. Bourouina and Y. Leprince-Wang, “Cell Refractive Index for Cell Biology and Disease Diagnosis: Past, Present and Future”, *Lab on a Chip*, Vol. 16, 2016.

88. Curry, T., R. Kopelman, M. Shilo and R. Popovtzer, “Multifunctional theranostic gold nanoparticles for targeted CT imaging and photothermal therapy”, *Contrast Media & Molecular Imaging*, Vol. 9, No. 1, pp. 53–61, 2014.

89. Liang, X., A. Liu, X. Zhang, P. Yap, T. Ayi and H. Yoon, “Determination of refractive index for single living cell using integrated biochip”, *The 13th International Conference on Solid-State Sensors, Actuators and Microsystems, 2005. Digest of Technical Papers. TRANSDUCERS ’05.*, Vol. 2, pp. 1712–1715 Vol. 2, 2005.

90. Sharan, P., S. M. Bharadwaj, F. Dackson Gudagunti and P. Deshmukh, “Design and modelling of photonic sensor for cancer cell detection”, *2014 International Conference on the IMpact of E-Technology on US (IMPETUS)*, pp. 20–24, 2014.

91. Zhang, L., Y. Zhang, Y. Hu, Q. Fan, W. Yang, A. Li, S. Li, W. Huang and L. Wang, “Refractive index dependent real-time plasmonic nanoprobes on a single silver nanocube for ultrasensitive detection of the lung cancer-associated miRNAs”, *Chemical Communications*, Vol. 51, pp. 294–297, 2015.

92. Yaroslavsky, A. N., R. Patel, E. Salomatina, C. Li, C. Lin, M. Al-Arashi and V. Neel, “High-contrast mapping of basal cell carcinomas”, *Optics Letters*, Vol. 37, No. 4, pp. 644–646, 2012.

93. Siegel, R. L., K. D. Miller, H. E. Fuchs and A. Jemal, “Cancer Statistics, 2021”, *CA: A Cancer Journal for Clinicians*, Vol. 71, No. 1, pp. 7–33, 2021.

94. Nichols, J. W. and Y. H. Bae, “EPR: Evidence and fallacy”, *Journal of Controlled*

Release, Vol. 190, pp. 451–464, 2014.

95. Wu, J., “The Enhanced Permeability and Retention (EPR) Effect: The Significance of the Concept and Methods to Enhance Its Application”, *Journal of Personalized Medicine*, Vol. 11, p. 771, 2021.

96. Zhang, Y.-R., R. Lin, H.-J. Li, W.-l. He, J.-Z. Du and J. Wang, “Strategies to improve tumor penetration of nanomedicines through nanoparticle design”, *WIREs Nanomedicine and Nanobiotechnology*, Vol. 11, No. 1, p. e1519, 2019.

97. Shi, Y., R. van der Meel, X. Chen and T. Lammers, “The EPR effect and beyond: Strategies to improve tumor targeting and cancer nanomedicine treatment efficacy”, *Theranostics*, Vol. 10, pp. 7921–7924, 2020.

98. Nakamura, Y., A. Mochida, P. L. Choyke and H. Kobayashi, “Nanodrug delivery: Is the enhanced permeability and retention effect sufficient for curing cancer?”, *Bioconjugate Chemistry*, Vol. 27, No. 10, pp. 2225–2238, 2016.

99. Kobayashi, H., R. Watanabe and P. L. Choyke, “Improving conventional enhanced permeability and retention (EPR) effects; what is the appropriate target?”, *Theranostics*, Vol. 4, No. 1, pp. 81–89, 2013.

100. Chauhan, V. P., T. Stylianopoulos, J. D. Martin, Z. Popović, O. Chen, W. S. Kamoun, M. G. Bawendi, D. Fukumura and R. K. Jain, “Normalization of tumour blood vessels improves the delivery of nanomedicines in a size-dependent manner”, *Nature Nanotechnology*, Vol. 7, No. 6, pp. 383–388, 2012.

101. Subhan, M. A., S. S. K. Yalamarty, N. Filipczak, F. Parveen and V. P. Torchilin, “Recent Advances in Tumor Targeting via EPR Effect for Cancer Treatment”, *Journal of Personalized Medicine*, Vol. 11, No. 6, p. 571, 2021.

102. Sani, A., C. Cao and D. Cui, “Toxicity of gold nanoparticles (AuNPs): A review”, *Biochemistry and Biophysical Report*, Vol. 26, No. 100991, p. 100991, 2021.

103. Sukhanova, A., S. Bozrova, P. Sokolov, M. Berestovoy, A. Karaulov and I. Nabiev, "Dependence of nanoparticle toxicity on their physical and chemical properties", *Nanoscale Research Letters*, Vol. 13, No. 1, p. 44, 2018.

104. Nel, A., T. Xia, L. Mädler and N. Li, "Toxic potential of materials at the nanolevel", *Science*, Vol. 311, No. 5761, pp. 622–627, 2006.

105. Dabrowski, J. M., *Chapter Nine - Reactive Oxygen Species in Photodynamic Therapy: Mechanisms of Their Generation and Potentiation*, Vol. 70 of *Advances in Inorganic Chemistry*, pp. 343–394, Academic Press, 2017.

106. Pan, Y., S. Neuss, A. Leifert *et al.*, "Size-Dependent Cytotoxicity of Gold Nanoparticles", *Small*, Vol. 3, No. 11, pp. 1941–1949, 2007.

107. Sani, A., C. Cao and D. Cui, "Toxicity of gold nanoparticles (AuNPs): A review", *Biochemistry and Biophysics Reports*, Vol. 26, No. 100991, p. 100991, 2021.

108. Pfaller, T., R. Colognato, I. Nelissen *et al.*, "The suitability of different cellular in vitro immunotoxicity and genotoxicity methods for the analysis of nanoparticle-induced events", *Nanotoxicology*, Vol. 4, No. 1, pp. 52–72, 2010.

109. Akhtar, M. J., M. Ahamed, S. Kumar *et al.*, "Nanotoxicity of pure silica mediated through oxidant generation rather than glutathione depletion in human lung epithelial cells", *Toxicology*, Vol. 276, No. 2, pp. 95–102, 2010.

110. Hnizdo, E. and J. Murray, "Risk of pulmonary tuberculosis relative to silicosis and exposure to silica dust in South African gold miners.", *Occupational and Environmental Medicine*, Vol. 55, No. 7, pp. 496–502, 1998.

111. Duan, J., Y. Yu, H. Shi *et al.*, "Toxic effects of silica nanoparticles on zebrafish embryos and larvae", *PLOS ONE*, Vol. 8, No. 9, p. e74606, 2013.

112. Stensberg, M. C., Q. Wei, E. S. McLamore *et al.*, "Toxicological studies on sil-

ver nanoparticles: challenges and opportunities in assessment, monitoring and imaging", *Nanomedicine*, Vol. 6, No. 5, pp. 879–898, 2011.

113. Prabhu, B. M., S. F. Ali, R. C. Murdock *et al.*, "Copper nanoparticles exert size and concentration dependent toxicity on somatosensory neurons of rat", *Nanotoxicology*, Vol. 4, No. 2, pp. 150–160, 2010.

114. Chen, H., A. Dorrigan, S. Saad, D. J. Hare, M. B. Cortie and S. M. Valenzuela, "In Vivo Study of Spherical Gold Nanoparticles: Inflammatory Effects and Distribution in Mice", *PLOS ONE*, Vol. 8, No. 2, pp. 1–8, 2013.

115. Ivanov, S., S. Zhuravsky, G. Yukina *et al.*, "In Vivo Toxicity of Intravenously Administered Silica and Silicon Nanoparticles", *Materials*, Vol. 5, No. 10, p. 1873–1889, 2012.

116. Ammari, H., M. Ruiz, S. Yu and H. Zhang, "Mathematical analysis of plasmonic resonances for nanoparticles: the full Maxwell equations", *Journal of Differential Equations*, Vol. 261, No. 6, pp. 3615–3669, 2016.

117. Lock, J. A. and G. Gouesbet, "Generalized Lorenz–Mie theory and applications", *Journal of Quantitative Spectroscopy and Radiative Transfer*, Vol. 110, No. 11, pp. 800–807, 2009.

118. Mätzler, C., "MATLAB Functions for Mie Scattering and Absorption Version 2", *IAP*, Vol. 8, 2002.

119. Yurkin, M. and A. Hoekstra, "The discrete dipole approximation: An overview and recent developments", *Journal of Quantitative Spectroscopy and Radiative Transfer*, Vol. 106, No. 1, pp. 558–589, 2007.

120. Olson, J., S. Dominguez-Medina, A. Hoggard, L.-Y. Wang, W.-S. Chang and S. Link, "Optical characterization of single plasmonic nanoparticles", *Chemical Society Reviews*, Vol. 44, No. 1, pp. 40–57, 2015.

121. Olson, J., S. Dominguez-Medina, A. Hoggard, L.-Y. Wang, W.-S. Chang and S. Link, "Optical characterization of single plasmonic nanoparticles", *Chemical Society Reviews*, Vol. 44, No. 1, pp. 40–57, 2015.

122. Lee, K.-C., S.-J. Lin, C.-H. Lin, C.-S. Tsai and Y.-J. Lu, "Size effect of Ag nanoparticles on surface plasmon resonance", *Surface and Coatings Technology*, Vol. 202, No. 22-23, pp. 5339–5342, 2008.

APPENDIX A: DIPOLE PLACEMENT FOR DIFFERENT NANOPARTICLE SHAPES

A.1. Nanospheres

Nanospheres are the simplest nanoparticle to model. A schematic of a nanosphere and the dipole model is presented in Figure A.1. The center of the particle is taken to be the origin point, as the particle is symmetric with respect to the origin point. The lower half of the sphere is defined as the symmetric points of (a, b, c) with respect to the origin where (a, b, c) is the dipole positions calculated by the process described in Section 2.5.

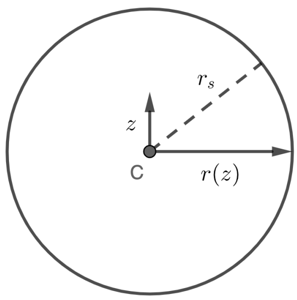

Figure A.1: Geometric Representation of a Nanosphere.

$r(z)$ of the sphere is calculated by

$$r(z) = \sqrt{r_s^2 - z^2}, \tag{A.1}$$

where r_s denotes the radius of the sphere.

A.2. Nanorods

Nanorods are very similar to nanospheres. A rod can be likened to an elongated sphere. Therefore, it maintains symmetry with respect to the origin. The same principles used in Section A.1 are used in the modeling of a rod. A schematic of a nanorod and the dipole model is presented in Figure A.2.

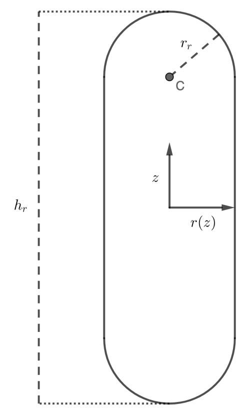

Figure A.2: Geometric Representation of a Nanorod.

$r(z)$ of the nanorod is calculated by

$$r(z) = \begin{cases} r_r, & \text{if } 0 < z < \frac{h_r}{2} - r_r \\ \sqrt{r_r^2 - (z - \frac{h_r}{2})^2} & \text{if } z > \frac{h_r}{2} - r_r, \end{cases} \tag{A.2}$$

where r_r denotes the radius of the rod, and h_r denotes the length of the rod.

A.3. Nanocones

Nanocones are more complex structures. Since they don't have an origin of symmetry, the origin point is taken at the base of the shape. A schematic of a nanocone and the dipole model is presented in Figure A.3. For simplicity, the cone is modeled in two separate parts, the smooth circular tip, and the slant.

The slant is the section of the cone where $r(z)$ decreases linearly. The maximum radius r_{max}, the minimum radius r_{min}, and the length of the slant h_{slant} can be

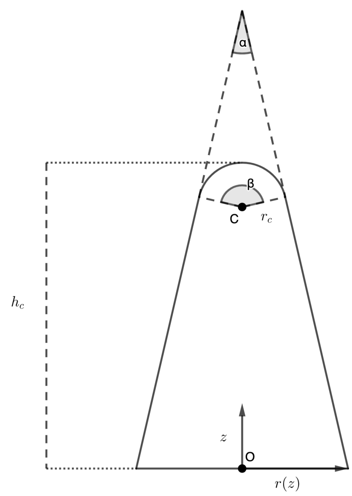

Figure A.3: Geometric Representation of a Nanocone.

calculated by

$$r_{min} = \frac{r_c}{cos(\alpha/2)}, \tag{A.3}$$

$$r_{max} = tan(\alpha/2)(h_c - r_c(1 - \frac{1}{sin(\alpha/2)}), \tag{A.4}$$

$$h_{slant} = h_c - r_c(1 - sin(\alpha/2)), \tag{A.5}$$

where r_c denotes the radius of the tip of the cone, h_c denotes the length of the cone, and α denotes the tip angle. If $r_c = 0$, the nanocone is described as having a sharp tip. Because of the definition of the slant section, $r(z)$ in the slant section of the nanocone is calculated by

$$r(z) = r_{max} - \frac{r_{max} - r_{min}}{h_{slant}} z \quad \text{if } 0 < z < h_{slant}, \tag{A.6}$$

$r(z)$ in the circular tip of the nanocone is calculated by

$$r(z) = \sqrt{r_c^2 - (z - h_{slant})^2} \quad \text{if } h_{slant} < z < h_c, \tag{A.7}$$

A.4. Bipyramid Nanoparticles

Bipyramid nanoparticles can be simply described as two pyramid-like nanoparticles attached from the ends. In this thesis, the bipyramid nanoparticles will be modeled as two nanocones. Therefore, dipoles of a bipyramid nanoparticle are calculated by simply combining two nanocones. The geometric representation of the shape is given in Figure A.4.

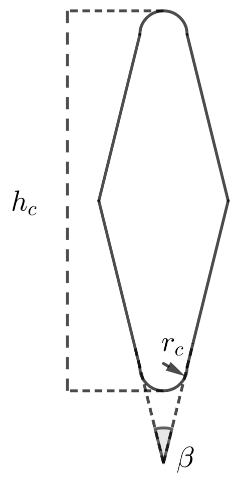

Figure A.4: Geometric Representation of a Bipyramid Nanoparticle.